





An innovative hematopoietic stem cell gene therapy approach benefits CLN1 disease in the mouse model

Marco Peviani^{1,2,3,4} , Sabyasachi Das¹ , Janki Patel¹, Odella Jno-Charles¹, Rajesh Kumar¹ , Ana Zguro¹, Tyler D Mathews¹, Paolo Cabras⁴, Rita Milazzo³, Eleonora Cavalca³, Valentina Poletti^{1,2}  & Alessandra Biffi^{1,2,5,*} 

Abstract

Hematopoietic stem and progenitor cells (HSPCs) can establish a long-lasting microglia-like progeny in the central nervous system of properly myeloablated hosts. We exploited this approach to treat the severe CLN1 neurodegenerative disorder, which is the most aggressive form of neuronal ceroid lipofuscinoses due to palmitoyl-protein thioesterase-1 (PPT1) deficiency. We here provide the first evidence that (i) transplantation of wild-type HSPCs exerts partial but long-lasting mitigation of CLN1 symptoms; (ii) transplantation of HSPCs over-expressing hPPT1 by lentiviral gene transfer enhances the therapeutic benefit of HSPCs transplant, with first demonstration of such a dose-effect benefit for a purely neurodegenerative condition like CLN1 disease; (iii) transplantation of hPPT1 over-expressing HSPCs by a novel intracerebroventricular (ICV) approach is sufficient to transiently ameliorate CLN1-symptoms in the absence of hematopoietic tissue engraftment of the transduced cells; and (iv) combinatorial transplantation of transduced HSPCs intravenously and ICV results in a robust therapeutic benefit, particularly on symptomatic animals. Overall, these findings provide first evidence of efficacy and feasibility of this novel approach to treat CLN1 disease and possibly other neurodegenerative conditions, paving the way for its future clinical application.

Keywords CLN1; hematopoietic stem cell gene therapy; lysosomal storage disorder; microglia

Subject Categories Genetics, Gene Therapy & Genetic Disease; Methods & Resources; Stem Cells & Regenerative Medicine

DOI 10.15252/emmm.202215968 | Received 4 March 2022 | Revised 25 January 2023 | Accepted 9 February 2023 | Published online 6 March 2023

EMBO Mol Med (2023) 15: e15968

Introduction

Neuronal ceroid lipofuscinoses (NCLs or CLNs) are a group of genetic disorders characterized by neurodegeneration and intracellular accumulation of an autofluorescent lipopigment (Mole & Williams, 2013). Together, they represent the most prevalent class of childhood neurodegenerative diseases. The NCLs encompass several distinct biological entities that vary in age at onset, specific neurological phenotype, and rate of progression. These entities share characteristic clinical features such as progressive vision loss, dementia, epileptic seizures, and loss of motor coordination, culminating in premature death. CLN1 disease, first described and one of the most frequent causes of NCL, is a lysosomal storage disorder (LSD) inherited in an autosomal recessive manner (Hawkins-Salsbury *et al*, 2013; Chandra *et al*, 2015). It is due to biallelic loss-of-function variants in the *PPT1* gene (also designated CLN1) encoding the lysosomal enzyme palmitoyl-protein thioesterase 1 (PPT1) that cleaves the thioester linkage of the fatty acid palmitate-to-cysteine residues of palmitoylated proteins (constituents of ceroid), a step that is necessary to allow degradation of these proteins by lysosomes. In most cases, CLN1 disease manifests clinically as infantile NCL (INCL) that is characterized by onset during childhood, at around 6–24 months of age, and has an invariably fatal outcome by 9–13 years of age (Santavuori *et al*, 1993). However, juvenile-onset and adult-onset forms of the disease have been described. Currently, no curative treatment is available that could prevent or reverse this fatal course.

The development of treatments for infantile CLN1 disease has been greatly accelerated by the availability of the *Ppt1*^{-/-} mouse model, where the murine gene coding for *Ppt1* has been knocked out (Gupta *et al*, 2001; Galvin *et al*, 2008). *Ppt1*^{-/-} mice recapitulate closely many phenotypic features observed in patients, including progressive motor disability (Gupta *et al*, 2001), visual impairment (Groh *et al*, 2014), muscle twitches, and recurrent seizures (Gupta

1 Gene Therapy Program, Dana-Farber/Boston Children's Cancer and Blood Disorders Center, Boston, MA, USA

2 Harvard Medical School, Boston, MA, USA

3 San Raffaele Telethon Institute for Gene Therapy (SR-TIGET), San Raffaele Scientific Institute, Milan, Italy

4 Department of Biology and Biotechnology "L. Spallanzani", University of Pavia, Pavia, Italy

5 Pediatric Hematology, Oncology and Stem Cell Transplant Division, Woman's and Child Health Department, University of Padova, Padova, Italy

*Corresponding author. Tel: +39 049 8218030; E-mail: alessandra.biffi@unipd.it

et al, 2001; Finn et al, 2013). At the histopathological level, they accumulate autofluorescent storage (AF) material in neurons and glial cells, show progressive neuronal loss (leading to thinning of the cortical layer) and prominent neuroinflammation (astrogliosis and microgliosis) (Gupta et al, 2001; Bible et al, 2004; Griffey et al, 2004; Kielar et al, 2007; Macauley et al, 2014).

Several therapeutic strategies have been tested in Ppt1^{-/-} mice with variable outcomes, including symptomatic treatments addressing the clinical manifestations of the disease, such as anti-excitotoxicity drugs (Finn et al, 2013); substrate reduction therapy exploiting cysteamine bis-tartrate or N-tert-butyl hydroxylamine (Gavin et al, 2013; Sarkar et al, 2013); or enzyme replacement therapy (Hu et al, 2012). In the latter case, insufficient widespread reconstitution of PPT1 activity in the CNS, including brain and spinal cord, is likely the key limitation that hindered successful clinical application by now. One major breakthrough has been recently reported at pre-clinical level by exploiting a gene therapy approach based on adeno-associated viral vectors (AAV) expressing the wild-type PPT1 administered in the cerebrospinal fluid in Ppt1^{-/-} mice (Shyng et al, 2017). However, as per most recent indications for the development of novel treatment options for LSDs, targeting secondary disease mechanisms, such as microglia activation and neuroinflammation, in addition to intervening on the primary disease culprit by compensating the enzymatic deficiency, is warranted for achieving robust therapeutic benefit (Groh et al, 2013; Macauley et al, 2014; Cavalca et al, 2018). In this setting, microglia cells, which are strongly implicated in the pathogenesis of LSDs, should be considered as a primary target cell type.

Hematopoietic stem cell gene therapy (HSC-GT) may successfully address this goal. Indeed, transplantation of genetically engineered hematopoietic stem and progenitor cells (HSPCs) in appropriate conditions can generate a microglia-like progeny that restores an efficient scavenging function within the whole CNS, with the potential to clear some of the accumulated substrates, reverse the detrimental effects of microglia activation due to the accumulation of undegraded substrate, and provide a new effective source of bioavailable enzyme within the CNS (Poletti & Biffi, 2019). Here, we provide the first proof of concept of therapeutic efficacy of HSC-GT in the CLN1 disease mouse model and exploit a newly developed CNS-targeting modality to further enhance its therapeutic effects.

Results

A novel disease severity scoring system accurately measures CLN1 disease symptoms in Ppt1^{-/-} mice

Identification of functional and clinically relevant pathologic readouts is instrumental to assess the efficacy of new therapeutic approaches. The motor function and behavioral assessments that include the rotarod and/or the open-field tests (Gupta et al, 2001; Griffey et al, 2004; Hu et al, 2012) to describe the Ppt1^{-/-} mice phenotype highlight significant deterioration of motor performance starting from around 210 days of age. Afterward, a very steep worsening of symptoms is observed, followed by a stable, poor performance up until the end stage of disease, with death occurring at around 245–260 days of age. At close examination, Ppt1^{-/-} mice display early symptoms starting from 140 to 150 days of age,

including popcorn seizures and jerks, abnormal displacement of hind- and/or fore-limbs when raised by the tail, alteration of the grooming behavior, that are not measured by the rotarod and open field tests. We, therefore, combined all these observations into a scoring system (see Appendix Fig S1A and Appendix Table S1) that provides a more comprehensive characterization of the phenotype of Ppt1^{-/-} mice from the early stages of disease progression. Given that the score increases with worsening of symptoms, we called it a disease severity score (DSS).

As shown in Appendix Fig S1B, wild-type (WT) mice never display DSS values higher than 1, whereas Ppt1^{-/-} mice show a DSS ~2 starting at ~160 days of age. A significant worsening of Ppt1^{-/-} mice symptoms then happens and by 190 days of age, animals display a rapid increase in DSS, followed by a progressive deterioration of the overall body condition up to 225 days, when they begin to reach the humane endpoint (HEP) (DSS ~6–7 on average). Rotarod testing conducted in parallel to DSS evaluation (Appendix Fig S1C) confirmed that the latter detects disease manifestations earlier than the former. Overall, based on DSS, we could identify three disease stages, characterized by specific behavioral and motor deficits, associated with the worsening of symptoms as the disease progresses (Appendix Fig S1D, Appendix Table S2): stage 1 or onset, defined by a DSS ≥ 2 at median age of 173 days; stage 2 or symptomatic phase, defined by a DSS ≥ 4 at median age of 205 days; and stage 3 or end stage, with a DSS ≥ 6 at median age of 229 days. We used this classification system to evaluate the effects of HSPC transplantation and HSC gene therapy in Ppt1^{-/-} mice.

Transplantation of WT hematopoietic cells attenuates the phenotype of Ppt1^{-/-} mice

To generate early feasibility data on HSPC transplantation in CLN1 disease, 6- to 8-week-old Ppt1^{-/-} mice were administered with busulfan (as myeloablative conditioning) and then transplanted intravenously (IV) with either unmanipulated total bone marrow (BM) or lineage negative (Lin⁻) HSPCs, corresponding to the CD34⁺ fraction in humans, retrieved from WT Ppt1^{+/+} donors (Appendix Fig S2A). To track donor-derived cells *in vivo*, Lin⁻ HSPCs were transduced with a lentiviral vector (LV) expressing the Δ.NGFR (nerve growth factor receptor) reporter gene, whereas for tracking BM cells, we relied on an allelic mismatch at the CD45 locus between donors (CD45.1) and recipients (CD45.2). As control groups, Ppt1^{-/-} mice were left untreated (UT) or were mock transplanted (namely underwent conditioning and transplantation of Ppt1^{-/-} unmanipulated, untransduced BM) to monitor the effects of conditioning on the disease. Starting at 140 days of age (85–100 days post-transplant), animals were assessed weekly for DSS to monitor disease progression. Mock-transplanted animals displayed an earlier symptom onset, with DSS > 2 already at 154 days of age (Fig 1A) and higher thereafter, and a shorter survival (median survival 228 vs. 248 days, respectively; *P* < 0.0001 log rank) compared to UT controls (Fig 1B). This could be due to the well-known intrinsic effects of the conditioning *per se* and of the pharmacological-grade busulfan formulation used for conditioning (BusilvexTM, Pierre Fabre Médicament) that contains dimethyl-acetamide (Hempel et al, 2007). Ppt1^{-/-} mice transplanted with WT BM or Lin⁻ cells displayed a milder disease progression than mock-transplanted and UT controls. Treated animals had DSS values below 4 up until

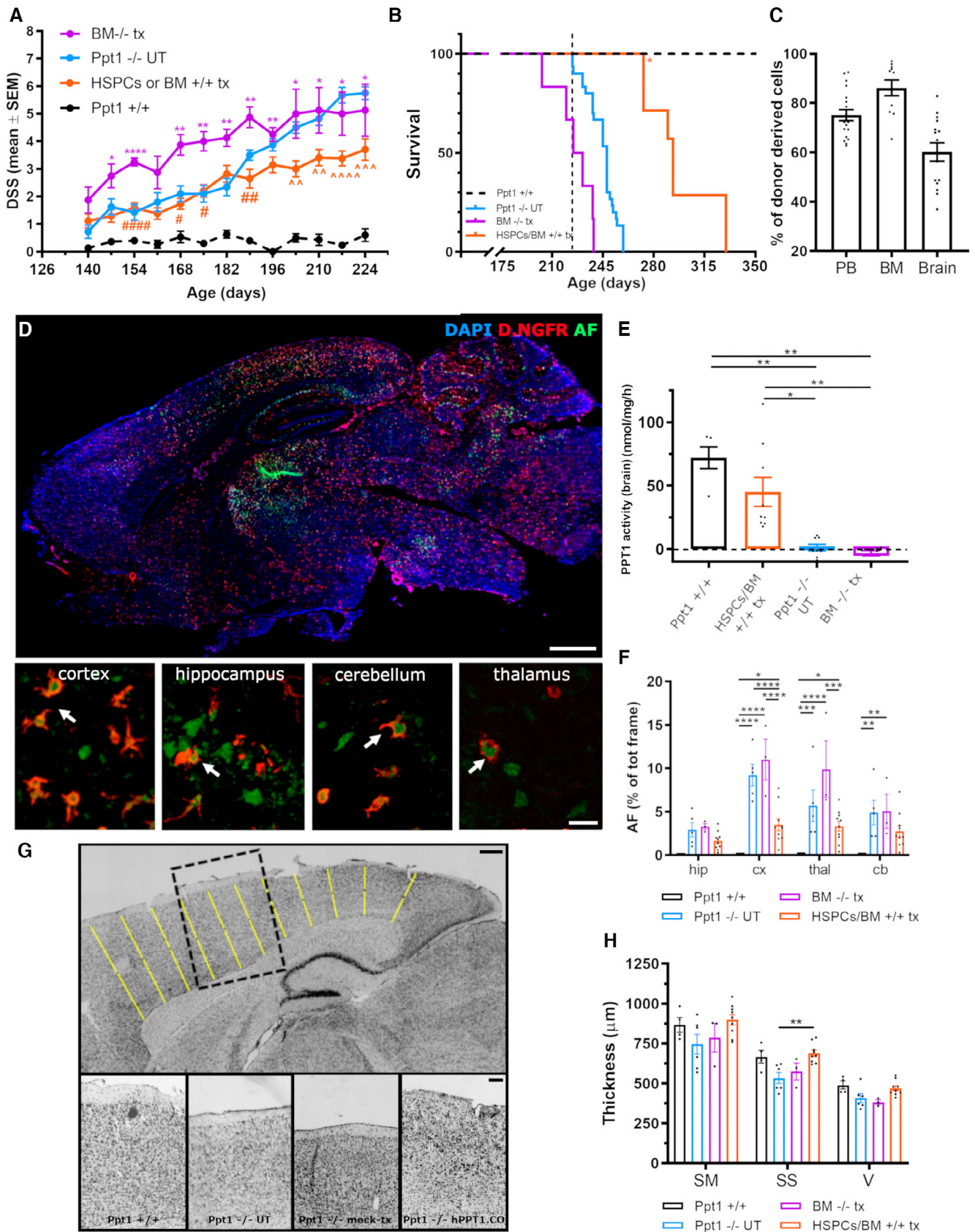


Figure 1.

Figure 1. Mild and long-lasting therapeutic effect of wild-type HSPCs/BM transplantation in Ppt1^{-/-} mice.

- A Ppt1^{-/-} mice transplanted with HSPCs or BM isolated from Ppt1^{+/+} mice display a milder disease progression, assessed by DSS, after onset of the symptoms, as compared to untreated or mock-transplanted Ppt1^{-/-} mice. Repeated measure ANOVA followed by Tukey's *post-hoc* test: **P* < 0.05; ***P* < 0.01; *****P* < 0.0001 vs. Ppt1^{+/+}; #*P* < 0.05; ##*P* < 0.01; ####*P* < 0.0001 vs. BM^{-/-} tx; ^*P* < 0.01; ^^*P* < 0.001; ^^*P* < 0.0001 vs. Ppt1^{-/-} UT.
- B Significant increase of survival in Ppt1^{-/-} animals transplanted with HSPCs or BM isolated from Ppt1^{+/+} mice; log-rank: HSPCs/BM^{+/+} tx vs. BM^{-/-} tx *P* < 0.001; BM^{-/-} tx vs. Ppt1^{-/-} UT *P* < 0.001.
- C Histograms showing the donor-cell chimerism in the peripheral blood (PB) at 60 days post-transplantation and in the BM or the brain, upon euthanasia at the end of the study.
- D Representative fluorescence microscope photomicrographs showing the distribution of donor-derived cells (transduced with ΔNGFR reporter gene, red) and autofluorescent storage material (AF, green) in the brain of a Ppt1^{-/-} mouse euthanized at 240 days of age, after transplantation with HSPCs isolated from Ppt1^{+/+} mice. Insets in (D) show high-magnification representative confocal scanning photomicrographs of ΔNGFR⁺AF⁺ cells in different regions of the CNS. Arrows show ΔNGFR⁺ cells engulfed with autofluorescent (AF) storage material. Scale bar (main figure) = 1 mm; scale bar (insets) = 25 μm.
- E Ppt1 enzymatic activity in the brain of untreated (Ppt1^{-/-}) or mock-transplanted (BM^{-/-} tx) mice or Ppt1^{-/-} animals transplanted with Ppt1^{+/+}-derived HSPCs or BM. The enzymatic activity in wild-type Ppt1^{+/+} mice is also reported as reference. **P* < 0.05; ***P* < 0.01; Kruskal–Wallis followed by Dunn's *post-hoc* test.
- F Quantification of autofluorescent storage material accumulation in different brain regions (hip = hippocampus, cx = cortex, thal = thalamus, and cb = cerebellum). **P* < 0.05; ***P* < 0.01; ****P* < 0.001; *****P* < 0.0001; two-way ANOVA followed by Tukey's *post-hoc* test. The histograms of Ppt1^{+/+} group are not visible in the graph as the AF signal was zero in these animals.
- G Representative brightfield photomicrographs of Nissl-stained brain sections from wild-type Ppt1^{+/+} mice and untreated or transplanted Ppt1^{-/-} mice. Black dashed box highlights a portion of the cortex, shown in the high-magnification insets. Yellow lines represent the segments applied to measure cortical thickness (see Materials and Methods for details on the quantification). Scale bar (main figure) = 1 mm; scale bar (insets) = 25 μm.
- H Histograms showing the quantification of cortical thickness. SM = somatomotor; SS = somatosensory; V = visual cortex. ***P* < 0.01; Kruskal–Wallis followed by Dunn's *post-hoc* test (for SM) or ANOVA followed by Tukey's *post-hoc* test (for SS and V).
- Data information: each histogram shows the mean ± SEM; the individual dots in each histogram represent one biological replicate. Source data are available online for this figure.

224 days of age (study termination, when the first UT-transplanted control died, dashed line in Fig 1B) and a significantly ameliorated DSS trajectory over time (Fig 1A). Disease progression was superimposable between Ppt1^{-/-} mice transplanted with Lin⁻ or BM WT cells (Appendix Fig S2B); thus, the two groups could be combined to highlight the overall clinical benefit exerted by the transplantation of Ppt1^{+/+} hematopoietic cells, in comparison with untreated and mock-transplanted Ppt1^{-/-} mice (Fig 1). Given the improved behavior of the transplanted mice, a small group of animals was kept alive (*n* = 7) for long-term observation to confirm that the disease remained mild (DSS below 6) beyond the natural disease course of Ppt1^{-/-} UT controls (of 230–237 days of age, on average). Except for two animals sacrificed early due to skin wounds (asterisk in Fig 1B), the remaining animals survived up to at least 280 days of age, with a DSS ≤ 5 (Appendix Fig S2B) and without limb stiffness. The last animals were finally euthanized at 330 days of age without reaching the HEP.

Average donor-cell chimerism, shortly after transplant (in peripheral blood, PB) and at sacrifice (BM and brain), was 80% in PB and BM and 55% within the brain CD11b⁺ myeloid compartment (Fig 1C, Appendix Fig S2C and D). Interestingly, there was widespread distribution of cells expressing ΔNGFR in the CNS of Ppt1^{-/-} recipients (Fig 1D), also in areas particularly affected by the pathology, such as the cortex, hippocampus, cerebellum, and thalamus (high-magnification insets in Fig 1D). In line with these data, the analysis of PPT1 activity on brain homogenates from mice treated with congenic (Ppt1^{+/+}) BM or HSPC cells confirmed a partial reconstitution of the enzymatic activity in the CNS of transplant recipients (Fig 1E, Appendix Fig S2E).

Autofluorescent (AF) storage accumulation in the CNS is a hallmark of CLN1 pathology, observed in humans and recapitulated in Ppt1^{-/-} mice (Gupta et al, 2001). Thus, we evaluated and measured the AF material on slices obtained from the brain (cortex, thalamus, hippocampus, and cerebellum) of transplanted and control mice sacrificed at the HEP or at 230–237 days of age. Ppt1^{-/-} UT and

mock-transplanted mice displayed a striking accumulation of AF material (Fig 1F), which was absent in WT mice. Treated animals showed an overall reduction in AF (Fig 1F, Appendix Fig S2F). Interestingly, the AF material was also present within the cell body of donor-derived cells in the four brain areas (cortex, hippocampus, cerebellum, and thalamus) that we analyzed (arrows in Fig 1D). Based on these results, we measured the cortical thickness on brain sections from treated and control animals colored with cresyl violet (Nissl) staining as readout of neuronal survival, and confirmed a rescue of neurons in the somatosensory cortex, and a tendency of increased thickness of the somatomotor and visual cortex of mice transplanted with Lin⁻ or total BM WT cells (Fig 1G and H and Appendix Fig S2G).

Transplantation of hPPT1-LV-transduced HSPCs significantly ameliorates the survival and the phenotype of Ppt1^{-/-} mice

Increasing up to above-normal levels the expression of the WT hydrolases in HSPCs (and their tissue progeny) by LV transduction represents an efficacious and clinically applicable approach for enhancing therapeutic efficacy of HSPC transplantation in mouse models and patients affected by other LSDs (Sessa et al, 2016). Therefore, we tested whether this concept would successfully apply also to CLN1 disease. A third-generation LV was generated encoding a codon-optimized human PPT1 cDNA under the control of the human phosphoglycerate-kinase (PGK) promoter (hPPT1-LV, Fig 2A) for transducing Ppt1^{-/-} Lin⁻ HSPCs (Visigalli et al, 2010). The transduced cells (1 × 10⁶ cells/mouse) were transplanted IV in young adult, 40- to 50-day-old, busulfan myeloablated Ppt1^{-/-} recipients. Given the toxicity observed upon usage of Busilvex™ in previous transplants, for these experiments we adopted a lab-grade (more tolerable) formulation of busulfan dissolved in acetone and peanut oil (Capotondo et al, 2012). As control groups, myeloablated Ppt1^{-/-} mice transplanted with cultured untransduced Ppt1^{-/-} HSPCs and untreated Ppt1^{-/-} animals were employed.

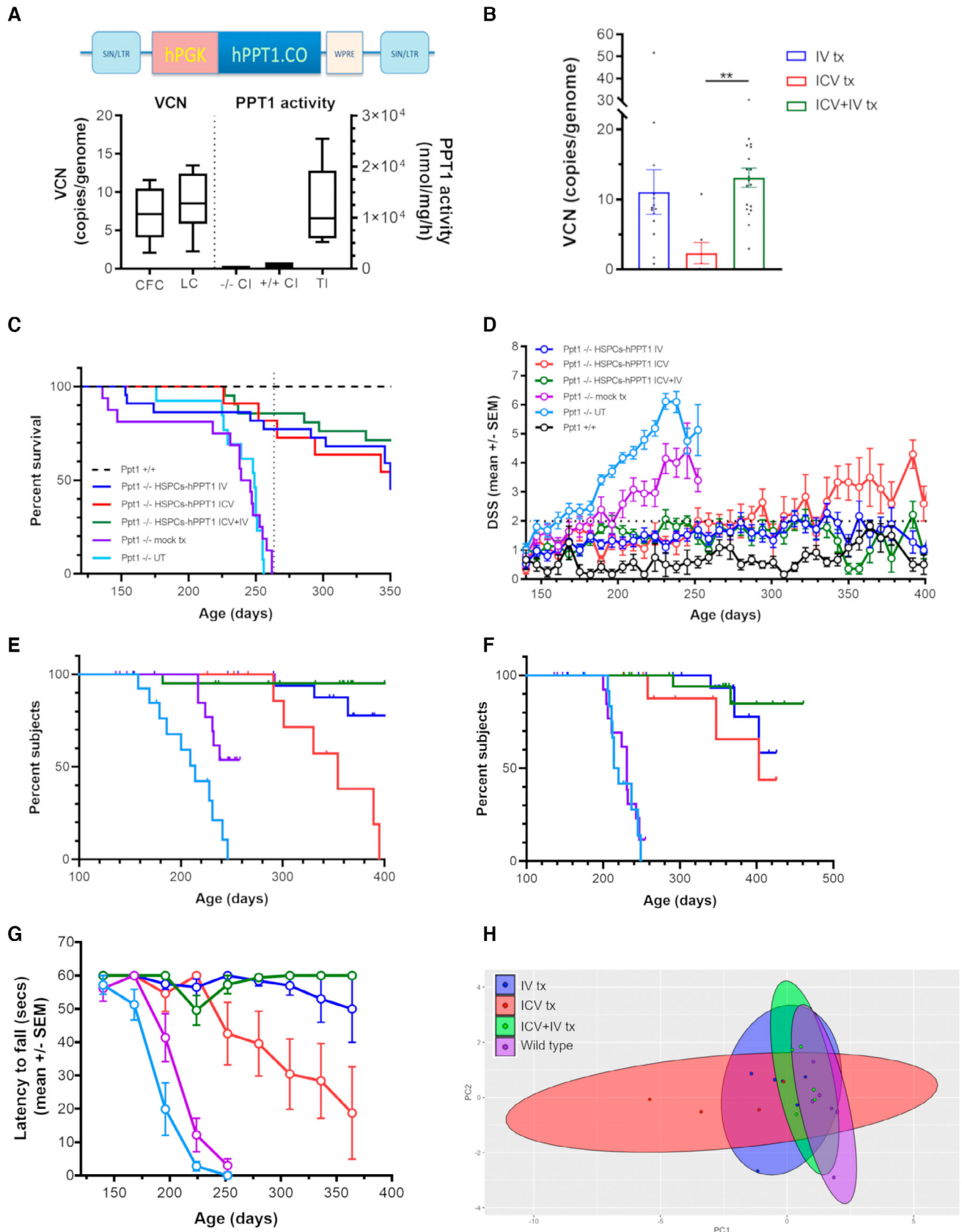


Figure 2.

Figure 2. Prevention of neurological deficits and increased survival of Ppt1^{-/-} mice transplanted with hPPT1-LV-transduced HSPCs.

- A High transduction efficiency of HSPCs assessed in colony-forming units and suspension cultures at 14 days after transduction with a lentiviral vector-expressing codon-optimized human PPT1 (left graph). Supraphysiological Ppt1 enzymatic activity in hPPT1-LV-transduced HSPCs as compared to Ppt1^{+/+} or Ppt1^{-/-} mock-transduced HSPCs (right graph).
- B High number of vector copies retrieved in peripheral blood (PB) of mice transplanted IV or IV+ICV with hPPT1-LV-transduced HSPCs. ***P* < 0.01. Kruskal–Wallis followed by Dunn's *post-hoc* test.
- C Significant increase of survival in Ppt1^{-/-} mice receiving the administration of hPPT1-LV-transduced HSPCs.
- D Long-lasting prevention of disease manifestations in Ppt1^{-/-} mice transplanted with hPPT1-LV-transduced HSPCs up to the study termination (around 360–400 days).
- E, F Significant prevention of pathological symptoms (DSS higher than 4 and limbs stiffness, respectively) in Ppt1^{-/-} mice transplanted with hPPT1-LV-transduced HSPCs.
- G Significant prevention of the deterioration of motor performances (assessed with rotarod) in Ppt1^{-/-} mice transplanted with hPPT1-LV-transduced HSPCs.
- H Principal component analysis (PCA) of combined behavioral data. Each dot in the graph represents one animal. The circles represent the overall distribution of each experimental group on the PCA plot, with respect to the other groups.

See Appendix Table S3 for detailed statistics of behavioral parameters shown in (C, E and F); see Appendix Table S4 for the statistical analysis of longitudinal DSS and Rotarod assessments shown in (D and G), respectively; see Appendix Table S5 for detailed statistics of the multivariate analysis on combined behavioral data. Data information: each histogram shows the mean ± SEM; the individual dots in each histogram represent one biological replicate. In boxplots (shown in A), the central band shows the median, the boxes represent the 25th and 75th percentile, whereas the whiskers show the minimum and maximum value of *n* = 10 biological replicates for VCN and *n* = 5 biological replicates for PPT1 activity. Source data are available online for this figure.

Myeloablated Ppt1^{+/+} WT animals transplanted with Ppt1^{+/+} HSPCs or untreated Ppt1^{+/+} mice were also included as reference during behavioral and biochemical assessments. After transplant, animals were monitored for survival and disease-associated phenotype until they reached the HEP or up to study termination.

High transduction efficiency of the Ppt1^{-/-} HSPCs was obtained with the newly developed LV (9 vector copies/genome on average), as measured on the output of the colony-forming assay (CFC) or of the liquid culture (LC) (assessed at 14 days after transduction, Fig 2A, left panel) of the batches used for *n* = 15 transplantations. This corresponded to an above-normal PPT1 activity in the LC from hPPT1-LV-transduced Ppt1^{-/-} HSPCs that reached ~20-fold of the enzymatic activity measured in the LC derived from Ppt1^{+/+} HSPCs (Fig 2A, right panel). Dose proof, defined as the evidence of actual engraftment of transplanted HSPCs in hematopoietic organs, was obtained 35–42 days after transplant by demonstrating high vector copy number (VCN) in the PB of transplanted animals (Fig 2B).

Animals transplanted intravenously (IV) with the hPPT1-LV-transduced HSPCs displayed a significantly increased survival as compared to UT or mock-transplanted Ppt1^{-/-} control mice (Fig 2C). Indeed, while all the UT and mock-transplanted animals reached HEP or were in poor body conditions due to the pathology by 260 days of age, 77% of the gene therapy-treated animals (17 of 22) were still alive at 260 days, and 68% of the initial cohort (15 of 22) survived until the study was terminated at ≥ 350 days of age. The recorded intercurrent deaths (ICDs) were mainly attributable to animals displaying poor body conditions in the absence of clinically relevant symptoms associated with CLN1 disease. This was further investigated by necropsy and histopathological assessments and the ICDs were generally not attributed to disease progression (Appendix Fig S5A) but rather to conditioning-related effects (Chanut *et al*, 2020).

Behavioral parameters were recorded on treated and control mice from 140 days of age until sacrifice (with a window of study termination that lasted from 350 to 500 days of age). Importantly, the weekly DSS assessment and monthly rotarod testing demonstrated that majority of the gene therapy-treated animals were protected from the development of severe symptoms of the disease, such as limb claspings, muscle atrophy, and stiffness. Indeed, while UT and mock-

transplanted animals experienced a progressive deterioration of their clinical conditions after the age of 220 days, with half of them in disease stage 2 (DSS ≥ 4) at 220–240 days of age (Fig 2D–F), most of the transplanted mice showed no clinical onset of the disease (DSS ≤ 2) for the whole duration of the observation (Fig 2D). Of the entire cohort of 22 treated mice, only 4 mice (18%) showed a mild pathology (DSS ≥ 4, Fig 2D and E) at study termination (by 350–360 days), and only three animals experienced a worsening of symptoms, identified as hindlimbs stiffness and 50% reduction of rotarod performance, after 320 days of age (Fig 2F and G).

Intra-CNS HSC gene therapy attenuates disease symptoms in Ppt1^{-/-} mice

We recently demonstrated that transplanting HSPCs directly in the cerebral lateral ventricles of busulfan-myeloablated recipients fosters reconstitution of the brain myeloid compartment by the transplanted cell progeny, leading to rapid, CNS-restricted engraftment of transplant-derived microglia-like cells (Capotondo *et al*, 2017). Thus, we assessed the therapeutic potential of hPPT1-LV-transduced HSPC administration directly in the cerebral lateral ventricles of myeloablated Ppt1^{-/-} recipients as a single treatment. This was done to understand whether CNS-restricted engraftment of the transduced, PPT1-expressing cells could be sufficient to alleviate CLN1 disease manifestations. Ppt1^{-/-} Lin⁻ HSPCs, transduced as described above with the PPT1-encoding LV, were transplanted (0.3 × 10⁶ cells/mouse) in the CNS by monolateral intracerebroventricular (ICV) injection in young adult, 40- to 50-day-old, busulfan-myeloablated Ppt1^{-/-} mice. Unmanipulated Ppt1^{-/-} BM cells were administered 5 days after ICV cell transplantation to aid hematopoietic rescue, as we do not expect significant contribution to hematopoiesis (no BM engraftment) of the ICV-injected cells (Capotondo *et al*, 2017). Animals treated by this CNS-directed approach (tot *n* = 10) showed an early benefit from the treatment, as 80% of them were alive and devoid of neurological symptoms (DSS < 2) at around 260 days of age, when all UT and mock-treated mice had already reached HEP (Fig 2C). However, later on, their behavioral assessment highlighted onset of symptoms and they became clearly

symptomatic with a DSS ≥ 4 (Fig 2D–F) and progressive motor deficits at rotarod (Fig 2G) by 300 days of age. In 3 of 10 animals from this group, hindlimbs stiffness was also observed starting from 340 days of age (Fig 2F) and a fraction of them reached HEP due to the pathology before study termination. By approximately 325 days of age, their survival dropped to 60% (Fig 2C).

Combined IV and ICV delivery of the transduced HSPCs enhances the efficacy of gene therapy leading to complete prevention of CLN1 disease symptoms

The severe and rapid progression of CLN1 disease in patients imposes the need for rapid and extensive restoration of the enzymatic activity in the CNS to increase the likelihood of preventing and/or halting disease manifestations. Based on the findings reported above, we tested the role of transduced HSPC delivery in the CNS as an additive strategy to enhance HSC-GT efficacy in a combinatorial (ICV+IV) transplant setting. This combined approach was intended at fostering and enhancing the myeloid CNS engraftment of the transplanted cells, the delivery of therapeutic enzyme to the CNS of Ppt1^{-/-} recipients, and the overall therapeutic potential of our treatment. Ppt1^{-/-} Lin⁻ HSPCs transduced with hPPT1-LV were transplanted in 40- to 50-day-old, busulfan-myeloablated Ppt1^{-/-} recipients, IV and ICV, as detailed above, on the same day, ≥ 24 h after the last busulfan dose. As control group, myeloablated Ppt1^{-/-} mice IV- and ICV-transplanted with cultured untransduced Ppt1^{-/-} HSPCs were employed.

Interestingly, the combinatorial ICV+IV treatment resulted in a robust therapeutic benefit with complete prevention of disease manifestations in the large majority of the treated mice. Indeed, 86% of the ICV+IV-transplanted animals (tot $n = 21$) were still alive at around 260 days of age (Fig 2C) and, despite their DSS, were different from untreated Ppt1^{+/+} mice, it was ≤ 2 and became ≤ 1 in the absence of any neurological symptoms at 350 days of age, resulting in significantly lower than the DSS shown by the IV or ICV-only group (Fig 2D). The 76% of ICV+IV-transplanted animals outlived controls and were sacrificed for study termination at 400–460 days of age with no evidence of disease manifestations (DSS ≤ 2 , no limb clasping or stiffness, preserved muscle tone) and full performance at rotarod test (Fig 2E–G).

We applied a principal component analysis (PCA) on the multiple behavioral parameters measured in each group (namely survival, DSS, and rotarod performance at 230, 330, and 350 days of age) that clearly showed a differential pattern of distribution of the affected versus WT control animals (Fig 2H). Interestingly, the distribution of the ICV+IV gene therapy-treated animals on the PCA plot was condensed and with a shape similar to WT control animals (Fig 2H). In contrast, animals transplanted with hPPT1-LV HSPCs via the IV-only or ICV-only routes showed a more scattered distribution on the plot that appeared as intermediate between the WT and PPT1^{-/-} distributions (Fig 2H). Multivariate analysis of variance and Hotelling's *t*-test confirmed a significant difference between animals transplanted ICV+IV and the animals that received the cells only IV or ICV, suggesting that the combinatorial transplant strategy could achieve greater (and more homogeneous across subjects) clinical benefit than the individual approaches (Appendix Table S5).

HSC gene therapy provides biochemical and pathological rescue of CLN1 disease: group comparison reveals an advantage of ICV+IV gene therapy over the other treatment approaches

To support the behavioral findings reported above, we investigated the CNS tissues of the gene therapy-treated and control animals from each group collected at study termination or when the mouse was euthanized. Robust engraftment of the transplanted cells was documented in the CNS of the gene therapy recipients as measured by quantification of integrated hPPT1-LV by ddPCR (vector copy number per cell) in the brain and spinal cord (Fig 3A). A higher VCN was measured in IV and ICV+IV groups as compared to ICV only in both brain and spinal cord. Importantly, a remarkable reconstitution of PPT1 activity was measured in the brain and spinal cord of gene therapy recipients, with two- to four-fold increase in enzyme activity above the physiological levels of Ppt1^{+/+} mice (Fig 3B). The highest PPT1 activity levels were measured in the brain of ICV+IV-transplanted mice (Fig 3B). Lower PPT1 activity was measured in the spinal cord, but not in the brain, of ICV- versus IV- and ICV+IV-transplanted mice (Fig 3B). IV- and ICV+IV-transplanted mice also had successful transduced cell engraftment (as measured by VCN) and robust PPT1 enzyme activity reconstitution in the BM (Fig 3C). As expected, negligible raise in PPT1 activity and transduced cell

Figure 3. Rescue of PPT1 activity and prevention of autofluorescence storage accumulation in the brain of Ppt1^{-/-} mice transplanted with hPPT1-LV-transduced HSPCs.

- A, B Vector copy number (VCN) and Ppt1 enzymatic activity assessed in brain and spinal cord of untreated or transplanted mice analyzed at study termination. * $P < 0.05$; ** $P < 0.01$; *** $P < 0.001$; **** $P < 0.0001$; Kruskal–Wallis followed by Dunn's *post-hoc* test.
- C VCN and hPPT1 activity retrieved in the BM of Ppt1^{-/-} transplanted with hPPT1-LV-transduced HSPCs IV, ICV, or ICV+IV, analyzed at study termination. ** $P < 0.01$; **** $P < 0.0001$; Kruskal–Wallis followed by Dunn's *post-hoc* test.
- D Quantification of autofluorescent (AF) storage material in different brain regions of untreated or transplanted mice analyzed at study termination. * $P < 0.05$; ** $P < 0.01$; *** $P < 0.001$; **** $P < 0.0001$; two-way ANOVA followed by Tukey's *post-hoc* test. The histograms of Ppt1^{+/+} group are not visible in the graph as the AF signal was zero in these animals.
- E Representative fluorescence microscope photomicrographs showing autofluorescent storage material (AF, green) in different brain regions of Ppt1^{-/-} mice transplanted with hPPT1-LV-transduced HSPCs at 400–420 days of age when the study was terminated. Mock-transplanted and untreated Ppt1^{-/-} mice at about 250 days, that is, humane endpoint, are shown as reference; 450-day-old untreated wild-type Ppt1^{+/+} mice are shown as control. NeuroTrace fluorescent Nissl staining (NT, red) is used to highlight neurons in different brain regions. Arrows highlight the surviving Purkinje cells in the cerebellum of IV- and ICV+IV-transplanted mice; arrowheads highlight the high number of AF⁺ cells in the Purkinje cell layer of ICV-transplanted or Ppt1^{-/-} untreated (UT) mice. Scale bar = 100 μ m.

Data information: each histogram shows the mean \pm SEM; the individual dots in each histogram represent one biological replicate. Source data are available online for this figure.

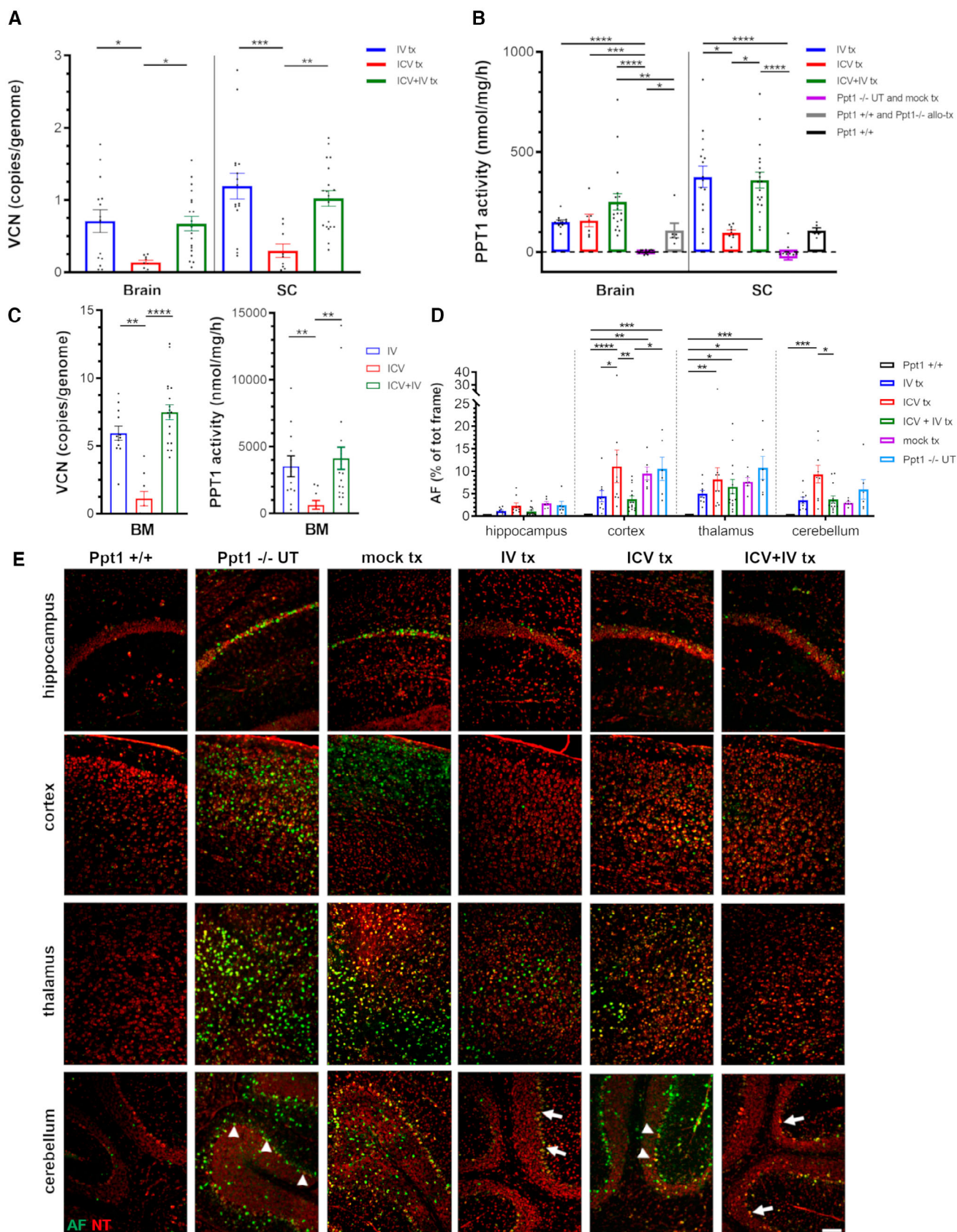


Figure 3.

engraftment were measured in the BM of ICV-transplanted animals, with exception of three animals displaying detectable VCN and PPT1 activities (Fig 3C), suggesting partial leakage from the ICV transplantation. The analysis of PPT1 protein distribution in the brain, measured by immunohistochemistry performed with an antibody specific for the human PPT1, highlighted a prominent and extensive distribution of the enzyme across all brain areas analyzed (namely hippocampus, cortex, thalamus, and cerebellum) for the IV- and ICV+IV-transplanted groups, whereas the ICV-transplanted animals displayed lower levels of PPT1 immunostaining, especially in the hippocampus and in the cerebellum (Appendix Fig S3A and graph in Appendix Fig S3B).

These findings correlated with evidence of sustained metabolic correction in the CNS of the treated animals. Indeed, treated animals showed clear-cut prevention of AF storage accumulation in the cortex, thalamus, and hippocampus, whereas in the cerebellum, storage material was not reduced for animals transplanted ICV (Fig 3D and E). In particular, in $Ppt1^{-/-}$ UT- and ICV-transplanted mice, we observed an accumulation of fluorescent material in the few surviving Purkinje cells (arrowheads in Fig 3E). In contrast, IV- and ICV+IV-transplanted mice displayed less prominent fluorescent material in Purkinje cells (arrows in Fig 3E). Consistent with these results, $Ppt1^{-/-}$ mice transplanted with hPPT1-LV HSPCs via IV or IV+ICV routes displayed significant protection from neuronal demise, resulting in a cortical thickness comparable to WT mice and significantly different from UT and mock-transplanted $Ppt1^{-/-}$ mice (Fig 4A). Notably, ICV-only transplanted animals showed a tendency to ameliorate without reaching statistical significance (Fig 4A).

Neuroinflammation is a hallmark of pathology in CLN1 disease (Groh et al, 2013; Macauley et al, 2014; Shyng et al, 2017). Early and progressive activation of microglia and astrocytes has been described in the $Ppt1^{-/-}$ mice, in brain areas critically affected by storage accumulation and neuronal demise. We investigated how the engrafted donor-derived cells affected the extent of glial reactivity by quantifying CD68 as a marker of microglia/macrophages. As expected, extensive CD68 immunoreactivity (characterized by many CD68⁺ amoeboid-like cells scattered throughout the parenchyma) was detected in the cortex, hippocampus, thalamus, and cerebellum of end-stage $Ppt1^{-/-}$ and mock-transplanted mice (arrows in Appendix Fig S4 and quantification in Fig 4B), consistent with the massive accumulation of AF storage material and severe neuronal loss that we reported in these regions (Fig 3D and E). In contrast, generally very few CD68⁺ cells were detected in the same regions of hPPT1-LV HSPCs-treated mice. Again, animals receiving the cells via either IV or ICV+IV routes displayed the greatest effect, with only few small CD68⁺ cells distributed sparsely throughout the parenchyma

(Appendix Fig S4). ICV+IV animals showed the lowest CD68 immunoreactivity of the entire analyzed cohort in the cortex (Fig 4B). A more pronounced CD68 immunoreactivity was instead observed in animals injected with hPPT1-LV HSPCs by the ICV-only route (Fig 4B), especially in the thalamus and cerebellum (arrowheads in Appendix Fig S4), suggestive of ongoing reactive gliosis in line with the AF storage accumulation and neuronal loss observed in these animals.

Principal component analysis was also applied on the multiple described histological parameters measured in each group (namely AF storage and CD68 immunoreactivity in cortex, thalamus, hippocampus, and cerebellum, and thickness of the cortical layer) with the aim of assessing the extent to which the different hPPT1-LV HSPC delivery routes affected these parameters. As shown in Fig 4C, animals transplanted with hPPT1-LV HSPCs IV and ICV+IV overall clustered in the proximity of $Ppt1^{+/+}$ healthy mice and far from mock-transplanted and untreated $Ppt1^{-/-}$ mice. However, while ICV+IV-transplanted mice showed the most homogenous clustering, suggestive of low variability, IV-transplanted mice showed scattered individuals. Multivariate analysis of variance and Hotelling's s^{-2} *t*-test confirmed that gene therapy-treated $Ppt1^{-/-}$ mice are significantly different from the $Ppt1^{-/-}$ UT group; among the gene therapy groups, animals transplanted ICV+IV or IV are significantly different from the ICV group (Appendix Table S5). Thus, while for ICV gene therapy the efficacy was only partial, especially in the long-term observation, a more robust rescue of the pathological CLN1 disease phenotype is obtained when hPPT1-LV HSPCs are transplanted IV or ICV+IV, the latter protocol providing a more homogeneous beneficial effect among the differently treated individuals.

Combined intra-CNS and IV gene therapy prolongs survival and alleviates the phenotype of symptomatic $Ppt1^{-/-}$ mice

Based on the information gained from this comparative study, we decided to treat with the hPPT1-LV HSPCs (administered IV or through the combined ICV+IV approach) $Ppt1^{-/-}$ mice at onset of symptoms, at 130 ± 15 days of age (Appendix Fig S1B), to verify whether we could achieve therapeutic benefit also in a stage of the disease when damage has already accumulated in the CNS. Animals received the standard pre-transplant busulfan-conditioning regimen and anti-seizure prophylaxis and the same dose of hPPT1-LV-transduced HSPCs as the young-adult mice that were transplanted in the previous experiments. To generate additional feasibility and toxicology data, in parallel to the gene therapy-treated $Ppt1^{-/-}$ animals, we also generated two large groups of mock-transplanted, $Ppt1^{-/-}$ and $Ppt1^{+/+}$ animals ($n = 21$ and $n = 24$,

Figure 4. HSC-GT rescues neuronal survival and mitigates microgliosis in $Ppt1^{-/-}$ mice.

- A Quantification of cortical thickness in the somatosensory (SS), somatomotor (SM), and visual (V) area, in untreated $Ppt1^{-/-}$ or $Ppt1^{+/+}$ mice, and in mice transplanted (tx) with hPPT1-LV-transduced HSPCs IV, ICV, or ICV+IV or mock transplanted analyzed at study termination. * $P < 0.05$; ** $P < 0.01$; *** $P < 0.001$; and **** $P < 0.0001$; Kruskal–Wallis followed by Dunn's *post-hoc* test.
- B Quantification of CD68 immunoreactivity in the cortex, hippocampus, thalamus, and cerebellum of untreated (UT) or gene therapy-treated $Ppt1^{-/-}$ mice. * $P < 0.05$; ** $P < 0.01$; *** $P < 0.001$; **** $P < 0.00001$; Kruskal–Wallis followed by Dunn's *post-hoc* test.
- C Principal component analysis of combined histopathological data. See Appendix Table S5 for detailed statistics of the multivariate analysis.

Data information: each histogram shows the mean \pm SEM; the individual dots in each histogram represent one biological replicate. Source data are available online for this figure.

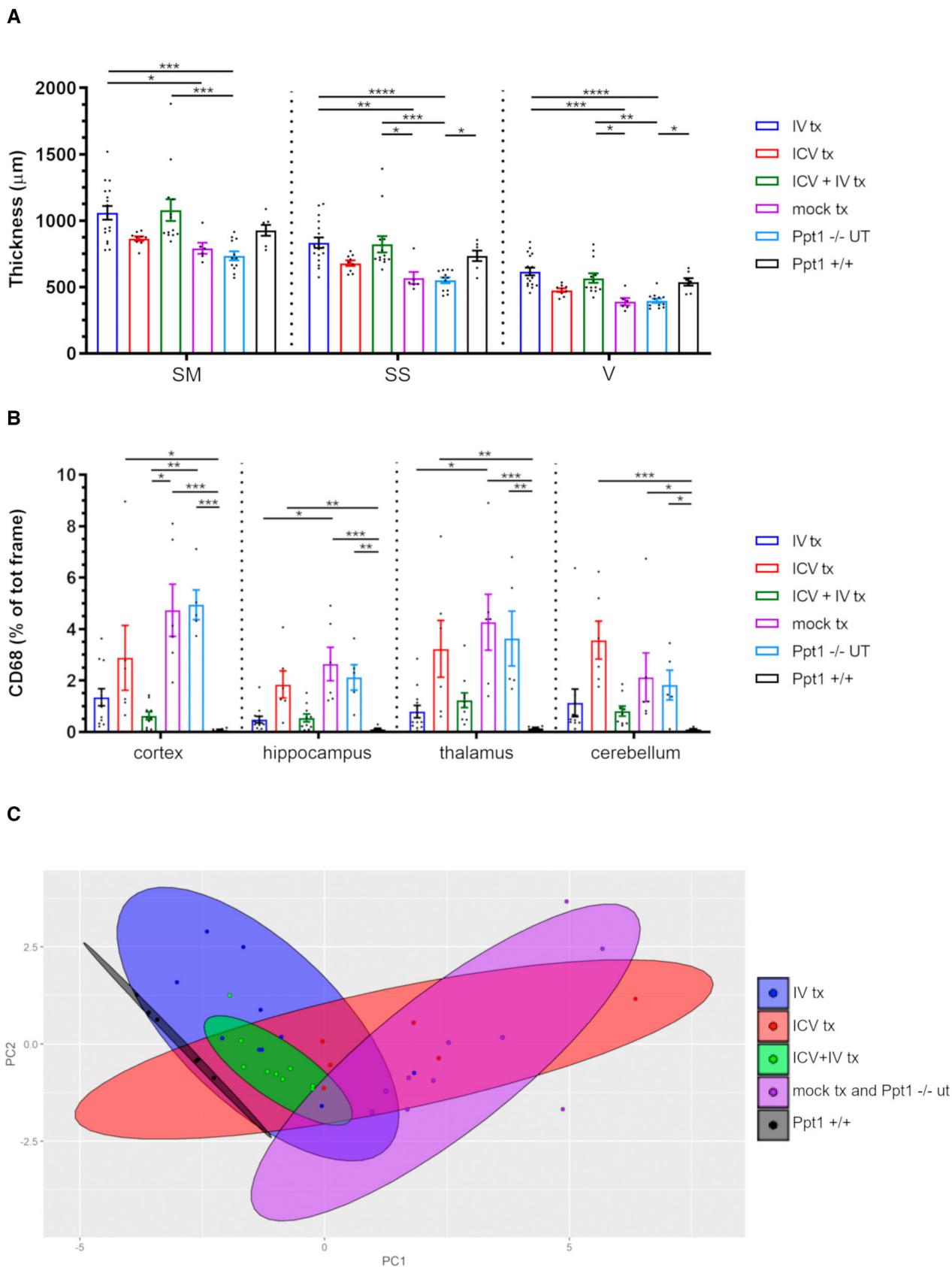


Figure 4.

respectively), which were exposed to the same busulfan-conditioning regimen, but transplanted with untransduced HSPCs (from Ppt1^{-/-} or Ppt1^{+/+} donors, respectively). Symptomatic mice transplanted IV or ICV+IV with the transduced HSPCs survived significantly longer than Ppt1^{-/-} UT and mock-transplanted mice, with about 80% of the treated animals still alive at 260 days of age, when all animals from Ppt1^{-/-} control groups had already died. Survival subsequently dropped also in treated mice, but the ICV+IV group showed a statistically greater survival probability than the IV one up to study termination (Fig 5A), indicating a more robust effect of gene therapy when the transduced cells were delivered also in the CNS. Interestingly, despite at medium term, the gene therapy-treated animals appeared broadly similar at behavioral testing to Ppt1^{-/-} UT and mock-transplanted mice (Fig 5B, Appendix Fig S5B); in the longer term, the pathology stabilized in the former (Appendix Fig S5B). Notably, 80% of gene therapy-treated animals never displayed hindlimbs stiffness (Fig 5C) which represents the most evident symptom displayed by Ppt1^{-/-} animals when they reach the advanced stage of the pathology. Consistent with these data, the analysis of donor-cell engraftment (measured as vector genome copies) performed at study termination confirmed high VCNs both in peripheral organs and in the CNS of the treated mice (Fig 5D, left graph). Interestingly, VCN in the BM and, most importantly, in the brain and spinal cord of ICV+IV-treated mice was higher than the VCN measured in IV-transplanted animals (Fig 5D). Accordingly, very high, above-normal PPT1 activity levels were detected in the CNS and BM of gene therapy-treated mice (Fig 5D, right graph). Of note, also in this case, ICV+IV cell transplantation was associated with a higher enzymatic activity in the brain (and BM) as compared to IV-treated animals (Figs 3B and 5D), confirming the advantage of combined cell delivery. The analysis of human PPT1 distribution in the brain of transplanted mice demonstrated a homogeneous high PPT1 immunostaining across all brain areas analyzed (Appendix Fig S3A and graph in Appendix Fig S3B). In line with these observations, gene therapy-treated animals displayed a prominent reduction of AF storage in the brain as compared to Ppt1^{-/-} untreated mice (Fig 5E and top graph in Fig 5F) and rescue of cortical thickness, with ICV+IV-transplanted mice showing a slightly better improvement in all the three areas analyzed (namely somatomotor, somatosensory, and visual cortex), as compared to the IV-transplanted mice (bottom graph in Fig 5F).

Safety of hPPT1-LV HSPCs transplantation in Ppt1^{-/-} mice

To collect information on the safety of the transplantation of hPPT1-LV HSPCs in Ppt1^{-/-} mice, the follow-up monitoring of the different experimental groups (treated, UT, and mock-transplanted PPT1^{-/-} and WT animals) consisted of twice weekly observation for viability and health status. Any intercurrent death (animal found dead or requiring euthanasia due to poor body condition) was registered and a full necropsy was performed. Moreover, we also monitored post-transplant and long-term hematopoiesis by evaluation of PB composition (through hemocytometric and FACS analysis) at 5–6 weeks post-transplant and at time of euthanasia, to verify the repopulation and multilineage differentiation of the transplanted HSPCs and to exclude the presence of clonal alterations or other hematopoietic anomalies.

As shown in Appendix Fig S5A, while the majority of Ppt1^{-/-} animals from the mock-transplanted and UT groups underwent euthanasia because they reached the pathological HEP, none of the Ppt1^{-/-} mice that were transplanted with hPPT1-LV HSPCs IV or ICV+IV had to be euthanized due to CLN1 disease symptoms. About 20% of animals from ICV-only group did require euthanasia because they reached the HEP. We reported in total 34 animals (spread across all groups, including mock-transplanted PPT1^{-/-} and WT mice, except the Ppt1^{-/-} UT) that had to be euthanized due to poor body conditions likely caused by abdominal ascites (confirmed by necropsy observation) and frequently accompanied by the presence of a solid tumor mass in the abdominal cavity (Appendix Table S6). Histopathological examination identified the tumor masses as sarcomas accompanied by atypical fibroplasia of the abdominal cavity. These sarcomas were attached to, and appeared to arise from, serosal/peritoneal surfaces (Appendix Table S7). One mass that was observed in Ppt1^{+/+} un-transplanted animals correlated with lymphoma and was considered to be related to a spontaneous tumor event that is reported to occasionally occur in wild-type C57BL/6J animals after 300 days of age (Frith *et al*, 1983; Wolf *et al*, 1988). The sarcomas were all similar in appearance and were diagnosed as sarcoma NOS (not otherwise specified) because they lacked collagen and were generally fairly pleomorphic. These findings were observed only in the groups that underwent busulfan conditioning, which is administered intraperitoneally, followed by transplantation of HSPCs (either transduced

Figure 5. Clinical benefit of HSC-GT in Ppt1^{-/-} mice transplanted at the symptomatic stage.

- A Significant increase in the survival of Ppt1^{-/-} mice transplanted at the symptomatic stage with hPPT1-LV-transduced HSPCs administered IV+ICV.
 B Similar progression of symptomatology in all treated groups until about 250 days of age.
 C Significant delay of the deterioration of motor performances (hindlimb stiffness) in Ppt1^{-/-} mice transplanted with hPPT1-LV-transduced HSPCs.
 D High vector copies (vector copy number—VCN, left panel) and increase in PPT1 enzymatic activity (right panel) in bone marrow (BM), brain, and spinal cord of mice transplanted with hPPT1-LV-transduced HSPCs. ****P* < 0.001; *****P* < 0.0001; Kruskal–Wallis followed by Dunn's *post-hoc* test.
 E Representative fluorescence microscope photomicrographs showing autofluorescent storage material (AF, green) in different brain regions of Ppt1^{-/-} mice transplanted with hPPT1-LV-transduced HSPCs at 18–20 weeks of age, analyzed at study termination. Ppt1^{-/-} mice mock transplanted at 18–20 weeks of age and analyzed at about 250 days, that is, humane endpoint, are shown as reference. NeuroTrace fluorescent Nissl staining (NT, red) is used to highlight neurons in different brain regions. Scale bar = 100 μm.
 F Top panel: quantification of autofluorescent (AF) storage material in different brain regions of untreated or transplanted mice analyzed at study termination. ***P* < 0.01; ****P* < 0.001; *****P* < 0.0001; two-way ANOVA followed by Tukey's *post-hoc* test. Bottom panel: histograms showing the quantification of cortical thickness. SM = somatomotor; SS = somatosensory; V = visual cortex. **P* < 0.05; ***P* < 0.01; *****P* < 0.0001; Kruskal–Wallis followed by Dunn's *post-hoc* test (for SM and V area) or ANOVA followed by Tukey's *post-hoc* test (for SS area).

See Appendix Table S3 for detailed statistics of behavioral data shown in (A, C and D).

Data information: each histogram shows the mean ± SEM; the individual dots in each histogram represent one biological replicate.

Source data are available online for this figure.

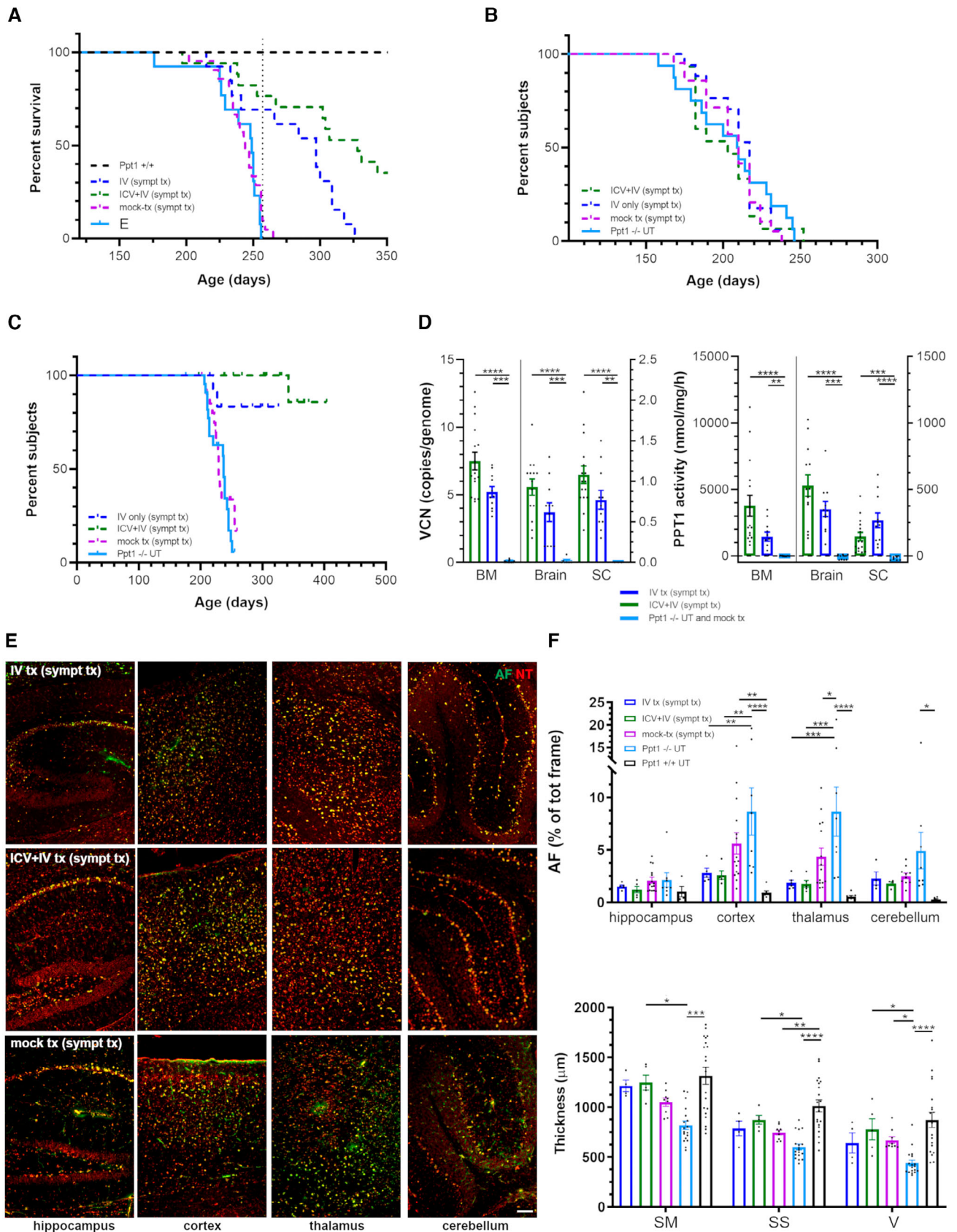


Figure 5.

or untransduced), and they occurred more frequently in animals that managed to survive longer than 260 days. In line with our observation, the toxicity associated with the route of administration of busulfan in mice must be intraperitoneal for technical reasons, which was reported in the context of other long-term observation pre-clinical studies (Chanut *et al*, 2020).

Overall, the hemocytometric and FACS analyses of PB did not highlight significant differences among groups at the first time point, suggesting that hematopoietic reconstitution occurred normally for all treated groups irrespective of the type of cells transplanted and the route of administration (Appendix Fig S5C). At euthanasia, normal PB composition was also documented, with the absence of hematopoietic anomalies in the treated and control groups (Appendix Fig S5D).

The histopathological analyses of hematopoietic organs, including spleen and BM, showed that Ppt1^{-/-} UT mice had decreased spleen size (subgross), decreased white pulp cellularity (W in Appendix Fig S6A), and increased apoptosis (arrowheads in Appendix Fig S6A), macrophage aggregates (asterisks in Appendix Fig S6A), and adipocytes (arrows in Appendix Fig S6A) when compared to Ppt1^{+/+} mice (Appendix Table S8); whereas in the BM, they had increased macrophage cellularity (arrows in Appendix Fig S6B, Appendix Table S9), suggesting that these findings represent overall a feature of the Ppt1^{-/-} strain. These findings were similarly observed in mock-transplanted Ppt1^{-/-} and in ICV-treated mice, whereas they were reduced in the animals that received hPPT1-LV-transduced HSPCs IV or ICV+IV (Appendix Fig S6A and B and Appendix Tables S8 and S9), supporting the beneficial effect exerted in the peripheral tissues by the functional hydrolase (Hu *et al*, 2012) released by the systemically transplanted hPPT1-expressing HSPCs. No hematopoietic clonal proliferations were observed.

Discussion

CLN1 disease is one of the most aggressive forms of NCL, still lacking a curative treatment. We and others demonstrated that HSC progeny cells can represent a vehicle for therapeutic molecule delivery to the CNS and exert neuroimmunomodulatory functions in the CNS upon transplantation in myeloablated host (Biffi *et al*, 2006; Visigalli *et al*, 2010; Sessa *et al*, 2016). For this reason, we here investigated whether HSC transplantation (HCT) and/or HSC-GT could determine widespread restoration of Ppt1 enzymatic activity throughout the nervous system and provide therapeutic benefit in the CLN1 disease animal model. To favor the establishment of a high donor-cell chimerism in the recipients' CNS (Lake *et al*, 1995; Macauley *et al*, 2012), we employed a busulfan-based conditioning regimen that is instrumental to foster efficient engraftment of donor-derived cells post-transplant (Capotondo *et al*, 2012). To accurately monitor the effects of our proposed therapeutic treatment, we developed a new clinical scoring system (called disease severity score—DSS) that enables precise highlighting of early signs of the disease and monitoring of the progressive behavioral deterioration of untreated Ppt1^{-/-} mice in parallel with other tests, such as the open-field test (Griffey *et al*, 2004) or the rotarod (our work and ref. Macauley *et al*, 2012), by which deficits become significantly evident only

at advanced disease stages when animals are already severely compromised.

Interestingly, standard WT HSC transplantation resulted in an unexpected clinical benefit. Indeed, transplant recipients exceeded in survival the natural disease course of Ppt1^{-/-} UT mice and developed only a mild disease phenotype up until the age of death of the first mock-transplanted control (224 days), with a mild DSS trajectory over time. *Ex vivo* analyses demonstrated high donor-cell chimerism both in hematopoietic cells and in brain CD11b⁺ myeloid/microglia cells. At the histological level, we observed a widespread distribution of the progeny of the transplanted cells throughout the brain parenchyma, including in the regions particularly susceptible to the disease, where the donor cells showed an activated phenotype and appeared engulfed with AF storage material. A partial restoration of Ppt1 enzymatic activity was observed in the brain of these animals at about 50% of the levels found in WT mice. This was sufficient to reduce (but not abrogate) the burden of AF material accumulation (especially in the thalamus and cortex) and prevent the thinning of the cortical layer, a hallmark of neurodegeneration in CLN1 disease. Notably, these data represent the first demonstration that HSC transplantation could be beneficial in CLN1 disease, provided that an optimized conditioning regimen is applied. The extension of survival and the rescue of histopathological disease hallmarks observed in the transplant recipients are similar, in extent, to the results described by other groups upon intracerebral injection of Ppt1 expressing adeno-associated viral (AAV) vectors (Griffey *et al*, 2006; Macauley *et al*, 2012, 2014). Notably, we transplanted 40- to 50-day-old Ppt1^{-/-} mice, when early signs of the pathology already started to appear (at least at the histopathological level). This suggests that the HSC-based approach retains great therapeutic potential also when it is applied at the early stages of neurodegeneration. Importantly, the evidence of donor-derived cells engulfed with storage material in several brain regions of the transplant recipients also suggests that the cell therapy approach could determine a benefit through a synergistic effect provided by the engagement of the HSC progeny not only in the release of the functional enzyme but also in the scavenging of toxic debris and storage from the environment.

Based on these findings, we hypothesized that gene transfer could increase the overall therapeutic potential of HCT also in CLN1 disease, as seen in other LSDs (Biffi *et al*, 2004; Visigalli *et al*, 2010). Indeed, multicopy LV gene transfer into Ppt1^{-/-} HSPCs could allow expression of Ppt1 enzyme above physiological levels in the transplanted cell progeny in tissues, including the nervous system, and therefore determine more robust clinical benefit. To address this hypothesis, busulfan-myeloablated Ppt1^{-/-} young adult recipients were transplanted IV with Ppt1^{-/-} HSPCs efficiently transduced with hPPT1-LV. This approach resulted not only in a significant increase in survival but also in a clearcut rescue of the CLN1 disease phenotype in the majority (approx. 80%) of the treated animals. In line with this observation, we reported supraphysiological levels of Ppt1 enzymatic activity in the brain and spinal cord of the transplanted mice (~3.5-fold higher than the WT or WT HSPC transplanted animals). This result was paralleled by high VCN retrieved in the CNS, further confirming that busulfan conditioning is instrumental to increase the efficiency of brain repopulation by the progeny of transplanted HSPCs. Cortical thinning was prevented, and AF storage accumulation was also reduced in the treated mice, as

compared to UT or mock-transplanted controls. The direct comparison of these results with the outcome of WT cell transplant clearly showed the superiority of gene therapy in preventing/arresting clinical and histopathological disease manifestations. Thus, we proved in the pre-clinical setting that the strategy that led to successful application of HSC gene therapy in children affected by other LSDs with primarily demyelinating features (Biffi *et al*, 2013; Sessa *et al*, 2016) could be efficacious also in CLN1 disease, which is a purely neurodegenerative condition.

In the attempt of enhancing further the therapeutic potential of HSC gene therapy for neurometabolic conditions and possibly extending treatment indication, we recently developed a novel approach based on the direct administration of the transduced HSPCs in the cerebral lateral ventricles (ICV delivery) of transplant recipients. This route *per se* or in combination with the standard IV cell delivery accelerates and fosters microglia reconstitution in busulfan-conditioned mice, particularly in the early post-transplant phase (Capotondo *et al*, 2017). This could represent a suitable strategy to anticipate timing of clinical benefit in neurometabolic diseases, especially for those pathologies like CLN1 disease where CNS damage is rapidly progressive and key to disease course. We, thus, tested the therapeutic efficacy of the transplantation of hPPT1-LV-transduced HSPCs ICV alone or in combination with IV delivery into busulfan-myeloablated Ppt1^{-/-} adult recipients. Interestingly, when the transduced HSPCs were delivered exclusively ICV, albeit with untransduced Ppt1^{-/-} hematopoietic cells transplanted IV to rescue the BM from myeloablation, we observed a significant therapeutic benefit, with increased survival and prevention of disease symptoms up to 250 days of age, when all the animals from the UT or mock-transplanted group had already died. This novel finding supports the concept that ICV transplantation of HSPCs could provide a significant benefit to CNS pathology and associated clinical deficits, a finding of potential value for other disorders where the CNS is the only affected tissue. However, the animals subsequently began to display some symptoms of CLN1 disease, including hindlimbs claspings and stiffness, and rotarod deficits. These deficits progressively worsened, but remained mild (DSS ~4), in approximately 40% of the treated animals. Moreover, despite histological and biochemical analyses at study termination showing restoration of enzymatic activity at WT levels in the brain and in the spinal cord of transplant recipients, AF storage was not homogeneously reduced as compared to control animals, and cortical thinning was not widely prevented. This partial benefit could be interpreted in light of different considerations. Firstly, even if CLN1 disease is considered an LSD with predominant CNS involvement, extra-CNS tissue alterations have been reported in affected patients and mice, such as cardiac dysfunction (Galvin *et al*, 2008) and metabolic deficits (Khaibullina *et al*, 2012). The accumulating deficits in these tissues are rarely detected due to the overwhelming symptomatology induced in the brain and spinal cord. We demonstrated that ICV-transplanted cells mainly repopulate the brain and spinal cord with a microglia-like progeny, with little to no engraftment in the extra-CNS and hematopoietic tissues. Thus, we can hypothesize that the ICV approach could have contributed to some rescue of the CNS pathology, as seen by the partial and initial effects, but not to halting extra-CNS manifestations that, once the lifespan was extended by the treatment, became evident and affected the disease course. This was also evidenced by histopathology performed on

hematopoietic organs. Moreover, we cannot exclude that partial exhaustion of the ICV-transplanted cells and/or of their progeny could have occurred in the long-term post-transplant. Indeed, at study termination, we detected lower VCN in the brain and spinal cord of ICV-transplanted mice as compared to the animals that received HSC gene therapy IV. This could be also due to competition between the ICV (transduced)-transplanted cells and the untransduced cells administered IV as a rescue from conditioning, or to a pathological CNS milieu disfavoring the engraftment of the ICV-transplanted HSPCs. Even if we did not test these hypotheses in our study, the evidence of ongoing inflammation and storage accumulation in the brain and spinal cord at time of transplant supports this view. Moreover, the biodistribution of ICV-transplanted HSPCs in the CLN1 disease mouse brain could be inefficient or uneven in some regions, which could explain the striking accumulation of AF storage in the cerebellum and the thalamus (consistent with the lower hPPT1 immunostaining observed in these regions, as compared with the other gene therapy groups). Similarly, limited engraftment in the spinal cord (paralleled by the lower Ppt1 activity retrieved in this compartment for the ICV-transplanted group) could be of relevance, as spinal cord pathology is considered of increasing importance in the Ppt1^{-/-} mouse (Shyng *et al*, 2017).

Based on these observations, we then decided to explore the therapeutic potential of combined (ICV and IV) administration of hPPT1 LV HSPCs. Importantly, the combined delivery of the transduced cells ICV and IV prevented disease manifestations and determined a long lasting and thorough prevention of symptoms, homogenous and substantial prevention of storage accumulation, and a widespread and broad prevention of cortical thinning, unlike that observed with the ICV-only approach. Notably, neuroinflammation, measured by signal intensity of the CD68 marker, was more substantially reduced in ICV+IV-treated mice compared to ICV-only recipients, suggesting a synergistic neuroprotective effect of the combined transplantation modality. These findings and the additive benefit of the combined ICV+IV HSC-GT therapy approach were supported by the PCAs and the multiparametric statistical analyses performed on all histological as well as all behavioral data. Indeed, at the behavioral level, the ICV+IV group displayed a statistically superior therapeutic potential as compared to the IV- and ICV-only approaches (from 350 days of age), whereas at the histological level, the ICV+IV was more similar to the IV-only group and both approaches displayed a statistical superior benefit as compared to the ICV-only group.

Finally, gene therapy was tested in late pre-symptomatic (130 ± 15 days old) animals to assess whether it could provide some benefit in such a challenging setting. Interestingly, gene therapy retained therapeutic efficacy, despite, as foreseeably, the overall treatment outcome being less impactful than in young-adult mice. Indeed, the IV- and ICV+IV-transduced cell transplantation in symptomatic mice resulted in high donor-cell chimerism and Ppt1 reconstitution in the brain and spinal cord, similar to young adult mice. The disease progressed slowly and with milder symptoms (substantial absence of hindlimbs stiffness) in symptomatic-treated mice compared to UT controls, resulting in significantly increased overall survival of the former compared to the latter. Notably, ICV+IV-treated mice significantly outlived not only the UT and mock-transplanted control mice but also the IV-treated cohort, further supporting the increased therapeutic potential of the former

approach. Thus, in this challenging setting of aged, symptomatic mice treatment, despite not being likely able to rescue already established CNS damage, HSC gene therapy, and in particular, the newly developed ICV+IV HSPC gene therapy approach, could prolong survival and delay disease manifestations of the affected mice, a remarkable result if compared to previously tested approaches that had resulted in therapeutic benefit only upon application to Ppt1^{-/-} newborns (Griffey et al, 2006; Macauley et al, 2012), and in line with the results obtained with AAV gene therapy upon intrathecal administration, a route that allows widespread reconstitution of Ppt1 activity along the neuraxis (Shyng et al, 2017). As per our previous and recent studies, the combined administration of HSPCs ICV+IV results in an overall enhancement of the myeloid donor chimerism in the brain and the spinal cord short term (45 days) after transplant (Capotondo et al, 2017; Milazzo et al, unpublished data). Thus, we can speculate that the value of combined IV and ICV delivery in the CLN1 setting, particularly, in symptomatic animals, likely relates to the ability of this approach to more rapidly impact the metabolic and neuroinflammatory defects associated with the disease.

As far as safety is concerned, busulfan conditioning was feasible in CLN1 disease mice (despite the well-known pro-epileptogenic potential of this drug) (Caselli et al, 2014), provided that anti-seizure prophylaxis (e.g., benzodiazepine) is administered before and during the conditioning. Necropsy, hemocytometric and histopathological assessments performed on the animals from all treated groups did not report any findings associated with the transplantation of transduced HSPCs; only few animals (spread across all transplanted groups) had to be euthanized due to poor body conditions associated with the development of ascites and sarcomas in the abdomen. This was likely due to the well-known long-term effects of busulfan (administered intraperitoneally diluted in a long-lasting solvent—see Materials and Methods) described also in other long-term studies. As far as the monitoring of possible genotoxicity related to vector integration in our experimental setting, normal hematopoietic system composition and histology of the bone marrow and spleen were observed, and no abnormal clonal proliferation events or actual tumors arising from the transplanted cells have been observed. As far as the safety of intraventricular HSPC administration is concerned, the extensive toxicological evaluation that was run in parallel to the efficacy assessments excluded tumor masses in the CNS in all study animals, including those in which the transduced HSPCs were administered ICV. To further support the safety of the intra-CNS transplantation of LV-transduced HSPCs, additional dedicated studies will be conducted on human HSPCs during the path to clinical translation.

In conclusion, our study provides first evidence that: (i) transplantation of wild-type HSPCs exerts a partial but long-lasting mitigation of the symptoms and could thus represent *per se* a valuable approach for CLN1 disease if applied in pre-symptomatic stage and upon a proper conditioning regimen; (ii) highly efficient gene transfer into the transplanted HSPCs enhances therapeutic benefit as compared to wild-type cell transplant in CLN1 disease as in other LSDs, with first demonstration of this dose–effect benefit for a purely neurodegenerative condition; (iii) transplantation of hPPT1 over-expressing HSPCs by the novel ICV approach is sufficient to transiently ameliorate CLN1 disease symptomatology in the absence of hematopoietic tissue engraftment of the transduced cells; and (iv) the combinatorial transplantation of transduced HSPCs intravenously

and ICV results in the most robust therapeutic benefit among the tested approaches on both pre-symptomatic as well as symptomatic animals, since it resulted in complete abrogation of the disease in a clinically relevant mouse model and determined a long-lasting and thorough prevention of symptoms. Notably, this same approach could uniquely benefit adult symptomatic animals, a finding of utmost importance for translation purposes. The clinical translatability of our strategy is further supported by the favorable safety profile we showed here.

Materials and Methods

Lentiviral vector expressing hPPT1 gene

Human codon-optimized PPT1 was synthesized by Genewiz and cloned into a pCCLsin.cPPT.humanPGK.Wpre vector by BamHI/Sall digestion. Lentiviral vectors were produced and titered according to previous published protocols (Visigalli et al, 2010).

In vivo experiments

Experiments were performed on B6.129S6-Ppt1tm1Hof/SopJ mice (hereafter called Ppt1^{-/-}), wild-type C57BL/6J mice, or B6.SJL-Ptprca Pepcb/BoyJ (hereafter called CD45.1 C57) mice, obtained from Jackson Lab, and maintained at San Raffaele Hospital or the Boston Children's Hospital animal research facility. The assignment of animals to experimental groups was done by applying randomization. The experiments involving animals abided by the ARRIVE Essential 10 guidelines.

Isolation and transduction of murine hematopoietic stem cells

Five- to eight-week-old Ppt1^{-/-}, wild-type C57BL/6J, or CD45.1 C57 donor mice were euthanized with CO₂, and BM was harvested by crushing the femurs, tibiae, humerus, and iliac crest. HSPCs were purified by Lineage- (Lin-) selection using the Miltenyi Biotec Lineage Cell Depletion Kit with magnetic separation with the autoMACS™ Separator, following manufacturer's instruction. Isolated Lin- were transduced using different lentiviral vectors (LVs) for 16 h at multiplicity of infection (MOI) 100 in stem span culture medium with antibiotics and cytokines (IL-3, IL-6, FLT-3, and SCF) at 37°C. The following LVs were used: pCCLsin.cPPT.humanPGK.ΔNGFR.Wpre (ΔNGFR-LV) for Lin- retrieved from wild-type C57BL/6J mice; pCCLsin.cPPT.humanPGK.human-codon-optimized-PPT1.Wpre (hPPT1-LV) for Lin- retrieved from Ppt1^{-/-} mice.

A fraction of the transduced cells were used for colony-forming assay to confirm the clonogenic potential as described (Visigalli et al, 2010), whereas another fraction of transduced cells were cultured for 14 days (Visigalli et al, 2010) in order to assess vector copy number by digital qPCR and transgene expression by flow cytometry (in the case of ΔNGFR-LV) or through PPT1 enzymatic activity assay (for hPPT1-LV).

Transplantation of murine hematopoietic stem cells

Six- to eight-week-old Ppt1^{-/-} or wild-type C57BL/6J mice were used as recipients of HSPCs transplantation. Before transplantation, mice were pre-treated with a myeloablative busulfan dose (27 mg/kg

i.p. for 4 consecutive days) in order to ensure a sustained CNS engraftment of the transduced cells. Seizures are well-recognized complications of high-dose busulfan therapy in clinical practice. Given the intrinsic higher susceptibility to seizures observed in CLN1 patients and recapitulated in Ppt1^{-/-} mice, we applied seizure prophylaxis by benzodiazepine in Ppt1^{-/-} animals undergoing busulfan administration as a strategy to reduce morbidity pre-transplant. The drug (diazepam) and administration protocol were defined based on literature evidence as follows: diazepam was administered for 10 days in drinking water, starting 2 days before the first busulfan administration. 0.25 mg/kg diazepam was administered for 8 days, followed by 2 days of wash-out with 50% consecutive reductions in the administered dose (0.125 and 0.063 mg/kg). Lin- cells were injected IV ($0.8\text{--}1.2 \times 10^6$ cells/mouse) or ICV ($0.2\text{--}0.4 \times 10^6$ cells/mouse) 24 h after the last busulfan administration. To ensure proper reconstitution of the hematopoietic system in animals undergoing busulfan conditioning and receiving only the ICV administration of HSPCs, a systemic IV administration of freshly isolated untransduced BM cells after lysis ($0.8\text{--}2.2 \times 10^6$ cells/mouse), hereafter defined as “support BM cells” (retrieved from Ppt1^{-/-} mice or from CD45.1 mice), was performed 5 days after ICV transplantation.

Intracerebroventricular administration was performed by surgery; briefly animals were anesthetized by isoflurane and mounted on a stereotaxic apparatus. Lin- cells (5 μ l/injection site) were injected monolaterally in the lateral ventricles with a 27G Hamilton syringe. Stereotaxic coordinates, referred to as Bregma, were AP: 0.5, L: -1.0 ; and DV: 2.5. After surgery, skin was sutured, and animals were returned to their cages for recovery. After transplant, mice were monitored with collection of clinical signs for early identification of intercurrent deaths (ICDs) 3 days/week. In the case of ICDs, proper assessments were conducted as described below. Intercurrent deaths up to day 31 are expected as a consequence of the conditioning regimen, therefore no specific analyses were performed for ICDs before 31 days post-transplant (body was kept in formalin). ICDs or mice sacrificed due to poor clinical conditions (> 15% weight loss and hunched posture) occurring from day 31 up to the end of study were processed, whenever feasible, in order to analyze the following parameters: (i) transduced and mock-transduced cell engraftment on bone marrow cells, any lesion and in brain and spinal cord samples; (ii) reconstitution of PPT1 activity on PBMCs or bone marrow cells, brain and spinal cord samples; and (iii) necropsy, histopathological and immunohistochemical examinations on a selected set of tissues. Moreover, dedicated assessments were scheduled at precise time intervals post-transplant:

i Dose proof at 5–7 weeks after transplantation

To assess proper hematopoietic reconstitution by the transplanted cell progeny, the following parameters were assessed: (i) transduced cell engraftment (VCN on bulk colonies grown from peripheral blood); and (ii) hematological parameters (complete blood count) on peripheral blood.

ii Behavioral assessment starting from 12 weeks after transplantation up to study termination

In order to monitor the effect of hematopoietic stem cell transplantation and the gene therapy treatment on disease progression

and survival, behavioral disease severity score assessment was performed weekly and animals were tested for rotarod performance once every 4 weeks. All behavioral analyses were performed in a blind manner.

Behavioral analyses

Disease severity score (DSS) was assigned by a trained operator blind. Several behavioral symptoms were summarized with a score that was proportional to the extent of disease severity (DSS ranging from 0, i.e., no symptoms, to 9, i.e., animal is in poor body conditions). The total score was obtained by summing up 1 point for each of the following symptoms detected: skin lesions or scratches, tail flick (abnormal tail posture), hind-limb or fore-limb muscle atrophy, abnormal hind-limb or fore-limb displacement when the animal is raised by the tail for maximum 15 s, hind-paws or fore-paws clasp behavior, and limbs stiffness.

Motor performance was assessed on constant speed rotarod. Animals were placed on a rotating bar (4 rpm, constant speed) for up to maximum 60 s. Time spent on the rotating bar was recorded in seconds. Animals falling from the rod before 60 s were returned to their cage for 5 min before repeating the test for a maximum of three trials. The best performance was recorded for subsequent analysis.

Behavioral analyses were performed by trained researchers blinded to the treatment group.

Mouse tissue collection and processing for flow cytometry and histology

Mice were euthanized under deep anesthesia by extensive intracardiac perfusion with cold PBS for 10 min after clumping the femur. Organs were then collected and differentially processed. Bone marrow (BM) cells were collected from the clumped femur as described. Brain and spinal cord were removed and divided into two longitudinal halves. For immunofluorescence and immunohistochemistry analysis, one half was fixed for 24 h in 4% PFA, embedded in OCT compound, and stored at -80°C , after equilibration in sucrose gradients (from 10 to 30%). One 1-mm-thick section of the other half of each tissue was fixed in formalin for histopathology. For flow cytometry analysis, cells from the not-fixed tissue were mechanically disaggregated to obtain a single cell suspension in 20 ml of GKN/BSA buffer (8 g/l NaCl, 0.4 g/l KCl, 1.42 g/l NaH₂PO₄, 0.93 g/l Na₂HPO₄, 2 g/l D+ glucose, and pH 7.4 + 0.002% BSA). Additionally, the spleen, thymus, liver, any lesion, sciatic nerves, and hindlimb muscles were carefully dissected and fixed in formalin for histopathology. The rest of the body was preserved in formalin for further investigations.

Flow cytometric analysis

Cells from BM and brain were analyzed by flow cytometry upon resuspension in blocking solution (PBS 5% FBS and 1% BSA) and labeling at 4°C for 15 min with the following specific antibodies: rat APC-Cy7 anti-mouse CD45 (BD Pharmingen) 1:100; rat APC anti-mouse CD11b (eBiosciences) 1:150; rat PE-Cy7 anti-mouse Ly-6C (BD Bioscience) 1:150; rat PE-Cy7 anti-mouse MHC.c.II (BD Bioscience) 1:150; and mouse Alexa447 anti-human human CD271 (NGF Receptor) (BD Pharmingen). For characterization of Lin- purity, the

following antibodies were used: rat APC anti-mouse CD11b (eBiosciences) 1:100; rat APC anti-mouse Gr-1 (BD Bioscience) 1:100; rat APC anti-mouse Ter119 (BD Bioscience) 1:100; rat APC anti-mouse CD3 (BD Bioscience) 1:100; rat APC anti-mouse B220 (BD Bioscience) 1:100; rat PE anti-mouse Sca-1 (BD Bioscience) 1:100; and rat PE-Cy7 anti-mouse c-kit (BD Bioscience) 1:100. For the exclusion of death cells, we used either 7-AAD (1 mg/ml) or DAPI (10 mg/ml) (Sigma-Aldrich). Cells were analyzed by LSR Fortessa (Beckton Dickinson).

Immunofluorescence and immunohistochemistry

Brains were serially cut in the sagittal plane on a cryostat in 14 μm sections; spinal cords were cut in the coronal plane in 20 μm sections. Tissue slides were washed twice with PBS, then sections were processed as follows:

CD271 (NGFR) staining

Sections were blocked with 0.3% Triton, 2% BSA, and 10% NGS (Vector Laboratories) for 1 h, then incubated O/N at 4C in a blocking buffer containing the mouse anti-human CD271 (BD Pharmingen) biotinylated primary antibody. Afterward, sections were washed three times with PBS and incubated for 30 min at RT with streptavidin-HRP (Perkin Elmer) dil. 1:100, washed, and finally, incubated for 8 min at RT with Tyramide-Cy5 (Perkin Elmer) dil. 1:300 in Amplification diluent (Perkin Elmer).

CD68 staining

Firstly, endogenous peroxidases were quenched by incubating the sections in 1% H_2O_2 in PBS for 10 min. Sections were blocked with 0.3% Triton and 10% FBS (Vector Laboratories) for 1 h, then incubated O/N at 4C in blocking buffer containing the rat anti-mouse CD68 (Abd Serotec) dil. 1:200, washed, and incubated for 1 h at RT with biotinylated anti-rat secondary antibody (Vector) dil. 1:200 in 1% FBS and PBS. Afterward, sections were washed three times with PBS and incubated for 1 h at RT with Avidin-Biotin complex (Vector) and then with DAB/ H_2O_2 mix (Sigma-Aldrich).

hPPT1 staining

Firstly, endogenous peroxidases were quenched by incubating the sections in 1% H_2O_2 in PBS for 10 min. Sections were blocked with 0.3% Triton and 10% FBS (Vector Laboratories) for 1 h, then incubated O/N at 4C in blocking buffer containing the mouse anti-human PPT1 (Novus Biologicals—Cat. No. NBP2-45388) dil. 1:500, washed, and incubated for 1 h at RT with biotinylated anti-mouse secondary antibody (Vector) dil. 1:200 in 1% FBS and PBS. Afterward, sections were washed three times with PBS and incubated for 30 min at RT with streptavidin-HRP (Perkin Elmer) dil. 1:100, washed, and finally, incubated for 8 min at RT with Tyramide-Cy5 (Perkin Elmer) dil. 1:300 in amplification diluent (Perkin Elmer). The specificity of the staining was confirmed by absence of any detectable signal on brain sections obtained from Ppt1^{-/-} mice.

NeuroTrace fluorescent Nissl staining

Sections were incubated for 10 min at RT in NeuroTrace 660 (Molecular Probes, Invitrogen) dil. 1:250 in PBS, then washed three times with PBS.

Nuclei were stained with DAPI (Sigma) 0.5 mg/ml in PBS. Slices were washed in PBS, air dried, and mounted with Mowiol.

Nissl staining was performed as previously described (Peviani et al, 2014).

Image acquisition and analysis

Sections stained by immunohistochemistry were acquired at a Nikon inverted microscope, whereas immunofluorescence was acquired at an epifluorescence Nikon inverted microscope or an SP5 Leica confocal microscope equipped with laser lines: Ar-Kr (488 nm), He-Ne green (532 nm), and a UV diode.

Cortical thickness was quantified on 10 \times tilescan pictures of the brain (at least two slices per sample) with Fiji software. Briefly, the length of 11 segments drawn perpendicular to the cortical meninges and evenly spaced throughout the full cortical surface (from visual to somatosensory and somatomotor cortex) was measured. An average of 3–4 segments per region was used in the analyses.

Autofluorescence (AF) storage material and hPPT1 staining were quantified on 10 \times epifluorescence images acquired in the FITC or Cy5 channel, respectively, in the cortex, hippocampus, thalamus, and cerebellum of each sample (at least two slices per animal and at least four images per brain region). Background was subtracted by Fiji software, then CellProfiler was used to identify the positive signal. Sections showing signs of bad tissue perfusion (such as the presence of erythrocytes in the blood vessels) were excluded from the analysis of the AF.

CD68⁺ signal was quantified by CellProfiler on 10 \times bright-field images taken from the cortex and hippocampus of each animal (at least two slices/mouse).

Ppt1 enzymatic activity assay

Enzymatic activity was measured according to published protocols (Griffey et al, 2004) on proteins extracted by six freeze-thaw cycles in saline (Visigalli et al, 2010) from cell pellets obtained from PB, BM, Lin- liquid cultures, or through homogenization by sonication (Macauley et al, 2012) from brain and spinal cord tissue. The activity was normalized to the total protein content of the specimen.

Statistical analysis

All statistical tests were two sided. Normality of the samples was first verified by applying Shapiro–Wilk test. Then, Student's *t*-test or Mann–Whitney non-parametric test was used for two-group comparisons. For comparisons with more than two groups, one-way ANOVA with Tukey *post-hoc* test (or Kruskal–Wallis non-parametric test followed by multiple-comparison corrected Dunn's test) was used; for multiple variable comparisons, two-way ANOVA was applied. In case of longitudinal behavioral data, repeated measures ANOVA was applied. Survival and end-points analysis were performed by log-rank test. Differences were considered statistically significant at a value of $*P < 0.05$, $**P < 0.01$, and $***P < 0.001$. In all figures with error bars, the graphs depict means \pm SEM. Statistical analyses were performed with GraphPad Prism v.9 software. Principal component analysis of combined behavioral or histological results and multivariate analysis of variance and Hotelling's *t*-test were performed using RStudio open-source software.

The paper explained

Problem

Neuronal ceroid lipofuscinosis (NCL) type 1 (or CLN1 disease) is one of the most aggressive and still incurable NCLs, characterized by progressive vision loss, dementia, epileptic seizures, and loss of motor coordination, culminating in premature death. The pathology is due to mutations in the PPT1 gene leading to insufficiency or loss of the lysosomal enzyme palmitoyl-protein thioesterase 1 (PPT1). The development of treatments for CLN1 disease has been greatly accelerated by the availability of the Ppt1^{-/-} mouse model, where the murine gene coding for Ppt1 has been knocked out. Ppt1^{-/-} mice recapitulate closely many phenotypic features observed in patients. However, despite several therapeutic strategies have been tested in Ppt1^{-/-} mice with variable outcomes, insufficient widespread reconstitution of PPT1 activity in the CNS, including brain and spinal cord, has been recognized as the key limitation that hindered successful clinical application till now.

Results

The transplantation of genetically engineered hematopoietic stem and progenitor cells (HSPCs) in appropriate conditions can generate a microglia-like progeny in the CNS that is capable of restoring an efficient scavenging function within the whole CNS with the potential to clear some of the accumulated substrates, reverse the detrimental effects of neuroinflammation induced by the accumulation of undegraded substrate and by the neurodegeneration, and provide a new effective source of bioavailable enzyme within the CNS. Here, we provide the first proof of applicability and therapeutic efficacy of hematopoietic stem cell (HSC) gene therapy in the CLN1 mouse model. Moreover, we exploit a newly developed CNS-targeted modality for HSPCs transplantation demonstrating that this route of cell delivery, combined with the systemic administration of HSPCs, provides long-lasting prevention of symptoms in young, pre-symptomatic animals and slows disease progression in aged CLN1 mice treated at a symptomatic stage. In parallel with the efficacy studies, we collected toxicological information to support the safety of the procedure in mice.

Impact

Overall, our pre-clinical results support the efficacy and feasibility of HSC gene therapy for the treatment of CLN1 disease and highlight the possibility to achieve a robust and long-lasting therapeutic effect by combining intra-CNS and systemic administration of HSPCs, particularly when HSC gene therapy is applied at the symptomatic stage.

Study approval

Procedures involving animals and their care were conducted in conformity with the institutional guidelines according to the international laws and policies (EEC Council Directive 86/609, OJ L 358, 1 Dec.12, 1987; NIH Guide for the Care and use of Laboratory Animals, U.S. National Research Council, 1996). The specific protocols covering the studies described in this study were approved by the Italian Ministry of Health, an internal Ethical Committee at San Raffaele Hospital, and the Boston Children's Hospital Institutional Animal Care and Use Committee.

Data availability

This study includes no data deposited in external repositories.

Expanded View for this article is available [online](#).

Acknowledgements

We acknowledge FRACTAL, Flow cytometry Resource (Milan), DFCI Flow Cytometry Core, Alembic of San Raffaele Hospital and DFCI Confocal Light Microscopy Cores, and the PASS-Bio Imaging facility of the University of Pavia and the Animal Behavior & Physiology Core of Boston Children's Hospital (in the person of Nick Andrews) for technical support. We wish to thank Danilo Pellin for assistance with statistical analyses and Vittorio Bertone for help with drafting the figures of the histological analyses. This work was supported by the following grants: ERC-2013-CoG, Project No 617162, and NIH R01 HD095935-04 to AB.

Author contributions

Marco Peviani: Data curation; software; formal analysis; supervision; investigation; visualization; methodology; writing – original draft; project administration; writing – review and editing. **Sabyasachi Das:** Investigation. **Janki Patel:** Investigation. **Odella Jno-Charles:** Investigation. **Rajesh Kumar:** Investigation. **Ana Zguro:** Investigation. **Tyler D Mathews:** Investigation. **Paolo Cabras:** Investigation. **Rita Milazzo:** Investigation. **Eleonora Cavalca:** Investigation. **Valentina Poletti:** Investigation. **Alessandra Biffi:** Conceptualization; data curation; formal analysis; supervision; funding acquisition; investigation; methodology; writing – original draft; project administration; writing – review and editing.

Disclosure and competing interests statement

AB and MP are co-authors in the patent PCT/US2017/056774. The authors have no other competing interests to declare. Synopsis Image was created with [Biorender.com](#).

For more information

- i <https://bdsrafoundation.org/what-is-batten-disease/>
- ii <https://rarediseases.org/rare-diseases/santavuori-disease/>
- iii https://www.orpha.net/consor/cgi-bin/OC_Exp.php?lng=EN&Expert=216

References

- Bible E, Gupta P, Hofmann SL, Cooper JD (2004) Regional and cellular neuropathology in the palmitoyl protein thioesterase-1 null mutant mouse model of infantile neuronal ceroid lipofuscinosis. *Neurobiol Dis* 16: 346–359
- Biffi A, De Palma M, Quattrini A, Del Carro U, Amadio S, Visigalli I, Sessa M, Fasano S, Brambilla R, Marchesini S *et al* (2004) Correction of metachromatic leukodystrophy in the mouse model by transplantation of genetically modified hematopoietic stem cells. *J Clin Invest* 113: 1118–1129
- Biffi A, Capotondo A, Fasano S, del Carro U, Marchesini S, Azuma H, Malaguti MC, Amadio S, Brambilla R, Grompe M *et al* (2006) Gene therapy of metachromatic leukodystrophy reverses neurological damage and deficits in mice. *J Clin Invest* 116: 3070–3082
- Biffi A, Montini E, Lorioli L, Cesani M, Fumagalli F, Plati T, Baldoli C, Martino S, Calabria A, Canale S *et al* (2013) Lentiviral hematopoietic stem cell gene therapy benefits metachromatic leukodystrophy. *Science* 341: 1233158
- Capotondo A, Milazzo R, Politi LS, Quattrini A, Palini A, Plati T, Merella S, Nonis A, di Serio C, Montini E *et al* (2012) Brain conditioning is instrumental for successful microglia reconstitution following hematopoietic stem cell transplantation. *Proc Natl Acad Sci USA* 109: 15018–15023

- Capotondo A, Milazzo R, Garcia-Manteiga JM, Cavalca E, Montepeloso A, Garrison BS, Peviani M, Rossi DJ, Biffi A (2017) Intracerebroventricular delivery of hematopoietic progenitors results in rapid and robust engraftment of microglia-like cells. *Sci Adv* 3: e1701211
- Caselli D, Rosati A, Faraci M, Podda M, Ripaldi M, Longoni D, Cesaro S, Lo Nigro L, Paolicchi O, Maximova N et al (2014) Risk of seizures in children receiving busulphan-containing regimens for stem cell transplantation. *Biol Blood Marrow Transplant* 20: 282–285
- Cavalca E, Cesani M, Gifford JC, Sena-Esteves M, Terreni MR, Leoncini G, Peviani M, Biffi A (2018) Metallothioneins are neuroprotective agents in lysosomal storage disorders. *Ann Neurol* 83: 418–432
- Chandra G, Bagh MB, Peng S, Saha A, Sarkar C, Moralle M, Zhang Z, Mukherjee AB (2015) *Cln1* gene disruption in mice reveals a common pathogenic link between two of the most lethal childhood neurodegenerative lysosomal storage disorders. *Hum Mol Genet* 24: 5416–5432
- Chanut FJA, Sanvito F, Ferrari G, Visigalli I, Carriglio N, Jofra Hernandez R, Norata R, Doglioni C, Naldini L, Cristofori P (2020) Conditioning regimens in long-term pre-clinical studies to support development of *ex vivo* gene therapy: review of nonproliferative and proliferative changes. *Hum Gene Ther* 32: 66–76
- Finn R, Kovács AD, Pearce DA (2013) Treatment of the *Ppt1*^{-/-} mouse model of infantile neuronal ceroid lipofuscinosis with the N-methyl-D-aspartate (NMDA) receptor antagonist memantine. *J Child Neurol* 28: 1159–1168
- Frith CH, Highman B, Burger G, Sheldon WD (1983) Spontaneous lesions in virgin and retired breeder BALB/c and C57BL/6 mice. *Lab Anim Sci* 33: 279–286
- Galvin N, Vogler C, Levy B, Kovacs A, Griffey M, Sands MS (2008) A murine model of infantile neuronal ceroid lipofuscinosis - ultrastructural evaluation of storage in the central nervous system and viscera. *Pediatr Dev Pathol* 11: 185–192
- Gavin M, Wen GY, Messing J, Adelman S, Logush A, Jenkins EC, Brown WT, Velinov M (2013) Substrate reduction therapy in four patients with milder *CLN1* mutations and juvenile-onset Batten disease using cysteamine bitartrate. *JIMD Rep* 11: 87–92
- Griffey M, Bible E, Vogler C, Levy B, Gupta P, Cooper J, Sands MS (2004) Adeno-associated virus 2-mediated gene therapy decreases autofluorescent storage material and increases brain mass in a murine model of infantile neuronal ceroid lipofuscinosis. *Neurobiol Dis* 16: 360–369
- Griffey MA, Wozniak D, Wong M, Bible E, Johnson K, Rothman SM, Wentz AE, Cooper JD, Sands MS (2006) CNS-directed AAV2-mediated gene therapy ameliorates functional deficits in a murine model of infantile neuronal ceroid lipofuscinosis. *Mol Ther* 13: 538–547
- Groh J, Kühl TG, Ip CW, Nelvagal HR, Sri S, Duckett S, Mirza M, Langmann T, Cooper JD, Martini R (2013) Immune cells perturb axons and impair neuronal survival in a mouse model of infantile neuronal ceroid lipofuscinosis. *Brain* 136: 1083–1101
- Groh J, Stadler D, Buttman M, Martini R (2014) Non-invasive assessment of retinal alterations in mouse models of infantile and juvenile neuronal ceroid lipofuscinosis by spectral domain optical coherence tomography. *Acta Neuropathol Commun* 2: 54
- Gupta P, Soyombo AA, Atashband A, Wisniewski KE, Shelton JM, Richardson JA, Hammer RE, Hofmann SL (2001) Disruption of *PPT1* or *PPT2* causes neuronal ceroid lipofuscinosis in knockout mice. *Proc Natl Acad Sci USA* 98: 13566–13571
- Hawkins-Salsbury JA, Cooper JD, Sands MS (2013) Pathogenesis and therapies for infantile neuronal ceroid lipofuscinosis (infantile *CLN1* disease). *Biochim Biophys Acta Mol Basis Dis* 1832: 1906–1909
- Hempel G, Oechtering D, Lanvers-Kaminsky C, Klingebiel T, Vormoor J, Gruhn B, Boos J (2007) Cytotoxicity of dimethylacetamide and pharmacokinetics in children receiving intravenous busulfan. *J Clin Oncol* 25: 1772–1778
- Hu J, Lu JY, Wong AMS, Hynan LS, Birnbaum SG, Yilmaz DS, Streit BM, Lenartowicz EM, Thompson TCM, Cooper JD et al (2012) Intravenous high-dose enzyme replacement therapy with recombinant palmitoyl-protein thioesterase reduces visceral lysosomal storage and modestly prolongs survival in a preclinical mouse model of infantile neuronal ceroid lipofuscinosis. *Mol Genet Metab* 107: 213–221
- Khaibullina A, Kenyon N, Guptill V, Quezado MM, Wang L, Koziol D, Wesley R, Moya PR, Zhang Z, Saha A et al (2012) In a model of Batten disease, palmitoyl protein thioesterase-1 deficiency is associated with brown adipose tissue and thermoregulation abnormalities. *PLoS One* 7: e48733
- Kielar C, Maddox L, Bible E, Pontikis CC, Macauley SL, Griffey MA, Wong M, Sands MS, Cooper JD (2007) Successive neuron loss in the thalamus and cortex in a mouse model of infantile neuronal ceroid lipofuscinosis. *Neurobiol Dis* 25: 150–162
- Lake BD, Henderson DC, Oakhill A, Vellodi A (1995) Bone marrow transplantation in Batten disease (neuronal ceroid-lipofuscinosis). Will it work? Preliminary studies on coculture experiments and on bone marrow transplant in late infantile Batten disease. *Am J Med Genet* 57: 369–373
- Macauley SL, Roberts MS, Wong AM, McSloy F, Reddy AS, Cooper JD, Sands MS (2012) Synergistic effects of central nervous system-directed gene therapy and bone marrow transplantation in the murine model of infantile neuronal ceroid lipofuscinosis. *Ann Neurol* 71: 797–804
- Macauley SL, Wong AMS, Shyng C, Augner DP, Dearborn JT, Pearce Y, Roberts MS, Fowler SC, Cooper JD, Watterson DM et al (2014) An anti-neuroinflammatory that targets dysregulated glia enhances the efficacy of CNS-directed gene therapy in murine infantile neuronal ceroid lipofuscinosis. *J Neurosci* 34: 13077–13082
- Mole SE, Williams RE (2013) Neuronal ceroid-lipofuscinoses. In *GeneReviews*[®] [Internet], Adam MP, Everman DB, Mirzaa GM, Pagon RA, Wallace SE, Bean LJH, Gripp KW, Amemiya A (eds). Seattle, WA: University of Washington. <https://www.ncbi.nlm.nih.gov/books/NBK1428/>
- Peviani M, Tortarolo M, Battaglia E, Piva R, Bendotti C (2014) Specific induction of *Akt3* in spinal cord motor neurons is neuroprotective in a mouse model of familial amyotrophic lateral sclerosis. *Mol Neurobiol* 49: 136–148
- Poletti V, Biffi A (2019) Gene-based approaches to inherited neurometabolic diseases. *Hum Gene Ther* 30: 1222–1235
- Santavuori P, Vanhanen SL, Sainio K, Nieminen M, Wallden T, Launes J, Raininko R (1993) Infantile neuronal ceroid-lipofuscinosis (INCL): diagnostic criteria. *J Inher Metab Dis* 16: 227–229
- Sarkar C, Chandra G, Peng S, Zhang Z, Liu A, Mukherjee AB (2013) Neuroprotection and lifespan extension in *Ppt1*^{-/-} mice by NtBuHA: therapeutic implications for INCL. *Nat Neurosci* 16: 1608–1617
- Sessa M, Lorioli L, Fumagalli F, Acquati S, Redaelli D, Baldoli C, Canale S, Lopez ID, Morena F, Calabria A et al (2016) Lentiviral haemopoietic stem-cell gene therapy in early-onset metachromatic leukodystrophy: an ad-hoc analysis of a non-randomised, open-label, phase 1/2 trial. *Lancet* 388: 476–487
- Shyng C, Nelvagal HR, Dearborn JT, Tynnelä J, Schmidt RE, Sands MS, Cooper JD (2017) Synergistic effects of treating the spinal cord and brain in *CLN1* disease. *Proc Natl Acad Sci USA* 114: E5920–E5929
- Visigalli I, Delai S, Politi LS, Di Domenico C, Cerri F, Mrak E, D'Isa R, Ungaro D, Stok M, Sanvito F et al (2010) Gene therapy augments the efficacy of

hematopoietic cell transplantation and fully corrects mucopolysaccharidosis type I phenotype in the mouse model. *Blood* 116: 5130–5139

Wolf NS, Giddens WE, Martin GM (1988) Life table analysis and pathologic observations in male mice of a long-lived hybrid strain ($A_f \times C57BL/6$) $F_{1\text{}}$. *J Gerontol* 43: B71–B78



License: This is an open access article under the terms of the [Creative Commons Attribution](#) License, which permits use, distribution and reproduction in any medium, provided the original work is properly cited.